

Theory of Charmless Inclusive B Decays and the Extraction of V_{ub}

BJÖRN O. LANGE^a, MATTHIAS NEUBERT^b, AND GIL PAZ^b

^a *Center for Theoretical Physics
Massachusetts Institute of Technology
Cambridge, MA 02139, U.S.A.*

^b *Institute for High-Energy Phenomenology
Newman Laboratory for Elementary-Particle Physics, Cornell University
Ithaca, NY 14853, U.S.A.*

Abstract

We present “state-of-the-art” theoretical expressions for the triple differential $\bar{B} \rightarrow X_u l^- \bar{\nu}$ decay rate and for the $\bar{B} \rightarrow X_s \gamma$ photon spectrum, which incorporate all known contributions and smoothly interpolate between the “shape-function region” of large hadronic energy and small invariant mass, and the “OPE region” in which all hadronic kinematical variables scale with M_B . The differential rates are given in a form which has no explicit dependence on the mass of the b quark, avoiding the associated uncertainties. Dependence on m_b enters indirectly through the properties of the leading shape function, which can be determined by fitting the $\bar{B} \rightarrow X_s \gamma$ photon spectrum. This eliminates the dominant theoretical uncertainties from predictions for $\bar{B} \rightarrow X_u l^- \bar{\nu}$ decay distributions, allowing for a precise determination of $|V_{ub}|$. In the shape-function region, short-distance and long-distance contributions are factorized at next-to-leading order in renormalization-group improved perturbation theory. Higher-order power corrections include effects from subleading shape functions where they are known. When integrated over sufficiently large portions in phase space, our results reduce to standard OPE expressions up to yet unknown $O(\alpha_s^2)$ terms. Predictions are presented for partial $\bar{B} \rightarrow X_u l^- \bar{\nu}$ decay rates with various experimental cuts. An elaborate error analysis is performed that contains all significant theoretical uncertainties, including weak annihilation effects. We suggest that the latter can be eliminated by imposing a cut on high lepton invariant mass.

1 Introduction

Good theoretical knowledge of strong-interaction effects in weak decays of B meson is crucial for a reliable exploration of the flavor sector of the Standard Model. In particular, the determination of the Cabibbo-Kobayashi-Maskawa (CKM) matrix elements $|V_{cb}|$ and $|V_{ub}|$ relies on an accurate description of bound-state effects in semileptonic decays. At present, the most precise calculations are available for inclusive semileptonic decays $\bar{B} \rightarrow X l^- \bar{\nu}$. Entries of the CKM matrix are complex numbers, most prominently V_{ub} and V_{td} , which leads to a wealth of phenomena such as CP violation. A graphical representation of this effect is the unitarity triangle, and a major effort of the B -physics community is underway to map out its apex. One of the biggest successes of this endeavor was the precise determination of the angle β , which has been measured with high accuracy from the time-dependent CP asymmetry in the $B \rightarrow J/\psi K_S$ decay channel [1]. The length of the side opposite the angle β is proportional to $|V_{ub}|$, and a high-precision determination of this quantity enables us to test the validity of the Standard Model and search indirectly for possible deviations from its predictions.

The theoretical tools for the calculation of inclusive B decays are QCD factorization on the one hand [2, 3, 4, 5, 6, 7], and local operator product expansions (OPE) on the other [8, 9]. Both approaches perform a systematic separation of non-perturbative quantities from perturbative ones, while organizing the calculation in inverse powers of the heavy b -quark mass m_b . The OPE is an appropriate tool for the calculation of total inclusive rates (for example in $\bar{B} \rightarrow X_c l^- \bar{\nu}$ decays) or for partial rates integrated over sufficiently large regions in phase space, where all components of the final-state hadronic momentum P_X^μ are large compared with Λ_{QCD} . QCD factorization, on the other hand, is better suited for the calculation of partial rates and spectra near kinematical boundaries, where typically some components of P_X^μ are large, while the invariant hadronic mass $M_X = \sqrt{P_X^2}$ is small. For example, any $\bar{B} \rightarrow X_u l^- \bar{\nu}$ event can be described with three independent kinematical variables, a useful choice of which is [7, 10]

$$P_l = M_B - 2E_l, \quad P_- = E_X + |\vec{P}_X|, \quad P_+ = E_X - |\vec{P}_X|. \quad (1)$$

Here P_\pm are the light-cone components of the hadronic final-state momentum along the jet direction, E_l is the charged-lepton energy, E_X is the jet energy, and \vec{P}_X is the jet momentum, all measured in the B -meson rest frame. In terms of these variables, the phase space is such that

$$\frac{M_\pi^2}{P_-} \leq P_+ \leq P_l \leq P_- \leq M_B, \quad (2)$$

with M_π being the mass of the lightest possible hadronic final state. The product $P_+ P_- = M_X^2$ is the hadronic invariant mass squared. In order to avoid large backgrounds from $b \rightarrow c$ transitions, all measurements of $|V_{ub}|$ are in one way or another restricted to the region of phase space where $P_+ P_- < M_D^2$. If the quantity P_- is allowed to reach its maximum value near M_B , it follows that P_+ is restricted to a region of order M_D^2/M_B , which is numerically comparable to Λ_{QCD} . This means that there are three parametrically different energy scales in the problem: the mass M_B of the initial state, the mass of the final hadronic state $\sim \sqrt{M_B \Lambda_{\text{QCD}}}$, and the low scale Λ_{QCD} at which perturbation theory breaks down and hadronic physics must be parameterized in terms of non-perturbative matrix elements. QCD factorization disentangles

the effects from these scales, so that the perturbative contributions can be expanded in powers of $\alpha_s(\mu_h)$ with $\mu_h \sim m_b$ (giving rise to “hard functions”) and $\alpha_s(\mu_i)$ with $\mu_i \sim \sqrt{m_b \Lambda_{\text{QCD}}}$ (giving rise to “jet functions”).

It is important to note that the heavy-quark expansions valid in these two kinematical regions are not identical, because the power counting rules differ in the two regimes. Also the nature of the nonperturbative inputs is different. In the OPE region, non-perturbative physics is encoded in a few hadronic parameters, and the heavy-quark expansion is the usual Wilsonian expansion in local operators. In the endpoint (or shape-function) region, the presence of multiple scales complicates the power counting, and the interplay between soft and collinear modes gives rise to large non-localities. As a result, non-perturbative physics is described by hadronic structure functions (called “shape functions”), and the heavy-quark expansion is an expansion in non-local string operators defined on the light-cone. The connections between the two regimes is that *moments* of the shape functions can be expressed in terms of local operators.

The goal of the present work is to develop a formalism that smoothly interpolates between the two kinematical regimes. This is essential for building an event generator for inclusive $\bar{B} \rightarrow X_u l^- \bar{\nu}$ and $\bar{B} \rightarrow X_s \gamma$ decays, which can be used to study differential decay rates and partial decay rates in different kinematical domains. In the shape-function region, our approach relies on exact QCD factorization theorems, which exist in every order of power counting. They allow us to systematically disentangle short- and long-distance physics and, in the process, resum parametrically large logarithms order by order in perturbation theory. This factorization can be done with high accuracy for the terms of leading power in $1/m_b$, and with somewhat less sophistication for the first-order power corrections. For the second-order power corrections, we only include contributions that do not vanish when integrated over all phase space. This is a safe approximation; the effects of the remaining $1/m_b^2$ terms can to a large extent be absorbed by a redefinition of the subleading shape functions arising at order $1/m_b$.

Our formalism is “optimized” for the shape-function region in the sense that a lot of sophisticated theoretical technology is applied in this regime. However, when our expressions for the differential decay rates are integrated over sufficiently wide domains, they automatically reduce to the simpler results that can be derived using the OPE approach, up to yet unknown terms of $O(\alpha_s^2)$. The moment relations for the shape functions are crucial in this regard. Note that local $1/m_b^2$ corrections in the OPE receive contributions from terms of leading power ($1/m_b^0$), subleading power ($1/m_b$), and sub-subleading power ($1/m_b^2$) in the shape-function region, so the transition is highly non-trivial. In implementing the program outlined here, we include all presently known information on the triple differential $\bar{B} \rightarrow X_u l^- \bar{\nu}$ decay rate and on the differential $\bar{B} \rightarrow X_s \gamma$ decay rate in a single, unified framework. We neglect, for simplicity, hadronic power corrections of order $1/m_b^3$ and higher, which are known to have a negligible effect on the observables considered here. The only possible exception is contributions from “weak annihilation”, which are estimated as part of our error analysis. We also ignore the existing results on $O(\beta_0 \alpha_s^2)$ radiative corrections, because they are only known for some single differential distributions, but neither for any double or triple differential $\bar{B} \rightarrow X_u l^- \bar{\nu}$ spectra, nor for the $\bar{B} \rightarrow X_s \gamma$ photon spectrum. While these corrections are sometimes found to be large when naive perturbation theory in $\alpha_s(m_b)$ is used, their effects are expected to be small

in our scheme, which is based on a complete scale separation using QCD factorization. We see no reason why they should be enhanced compared with other, unknown corrections of $O(\alpha_s^2)$.

A technical complication in realizing the approach described here has to do with the treatment of phase-space factors. The heavy-quark expansion of the hadronic tensor for $\bar{B} \rightarrow X_u l^- \bar{\nu}$ decay gives rise to expressions that are singular at certain points in phase space. One way to avoid these singularities is to also expand phase-space factors order by order in $1/m_b$ (see, e.g., the treatment in [11]). However, since this expansion depends on the kinematical cuts of any given analysis, it cannot be implemented in a straightforward way in an event generator. An alternative is to reorganize the heavy-quark expansion in such a way that the expansion parameter is related to *hadronic* (as opposed to *partonic*) kinematical variables, in which case kinematical singularities are always canceled by exact phase-space factors. Following this strategy, we obtain expressions for decay distributions and partial decay rates which are free of explicit reference to partonic quantities such as the b -quark mass. A dependence on m_b enters only implicitly via the first moment of the leading-order shape function denoted by $\hat{S}(\hat{\omega})$. The philosophy of our approach is that this function¹ is extracted experimentally from a fit to the $\bar{B} \rightarrow X_s \gamma$ photon spectrum, which has been measured with increasing precision in the region where $P_+ = M_B - 2E_\gamma \sim \Lambda_{\text{QCD}}$. This is analogous to the extractions of parton distribution functions from deep inelastic scattering. The photon spectrum is experimentally accessible to energies as low as 1.8 GeV, which corresponds to a sampling of the shape function for values of $\hat{\omega}$ up to around 1.7 GeV. Once the shape function has been extracted over this range, we can use it to obtain predictions for arbitrary partial $\bar{B} \rightarrow X_u l^- \bar{\nu}$ decay rates with cuts. In doing so, the residual hadronic uncertainties in the extraction of $|V_{ub}|$ only enter at the level of power corrections.

The paper is structured as follows: In Section 2 we collect the relevant formulae for the calculation of the $\bar{B} \rightarrow X_s \gamma$ photon spectrum. These expressions can be used to extract the leading non-perturbative structure function from experiment. An analogous presentation for the triple differential decay rate in $\bar{B} \rightarrow X_u l^- \bar{\nu}$ decays is given in Section 3. In order to perform a numerical analysis one needs to rely on parameterizations of the shape functions. A collection of several useful functional forms is given in Section 4. In Section 5 we present a full error analysis of partial $\bar{B} \rightarrow X_u l^- \bar{\nu}$ decay rates for a variety of experimental cuts. We also explore the sensitivity of the results to the b -quark mass and to the functional forms adopted for the shape functions. Section 6 contains our conclusions.

2 Inclusive radiative decays

The decay process $\bar{B} \rightarrow X_s \gamma$, while more complex in its short-distance physics, is considerably simpler in its kinematics than the semileptonic process $\bar{B} \rightarrow X_u l^- \bar{\nu}$. Since the radiated photon is on-shell, the hadronic variables P_\pm that describe the momentum of the X_s system are trivially related to the photon energy E_γ by $P_+ = M_B - 2E_\gamma$ and $P_- = M_B$. In the crudest approximation, namely at tree level and leading power, the photon-energy spectrum is directly

¹More precisely, we define a new shape function $\mathcal{S}(\hat{\omega})$ by the combination of leading and subleading shape functions contributing to $\bar{B} \rightarrow X_s \gamma$ decay, and we will use the same function to make predictions for $\bar{B} \rightarrow X_u l^- \bar{\nu}$ decay distributions.

proportional to the leading shape function, $d\Gamma_s/dE_\gamma \propto \hat{S}(P_+)$. In this section we collect all relevant formulae needed to compute the $\bar{B} \rightarrow X_s \gamma$ photon spectrum (or, equivalently, the invariant hadronic mass distribution). Our notation is adopted from [7, 11]: hatted shape functions are defined on the interval $\hat{\omega} \in [0, M_B]$.

The differential decay rate can be written as

$$\frac{d\Gamma_s}{dE_\gamma} = \frac{G_F^2 \alpha}{2\pi^4} E_\gamma^3 |V_{tb} V_{ts}^*|^2 \overline{m}_b^2(\mu_h) |C_{7\gamma}^{\text{eff}}(\mu_h)|^2 U(\mu_h, \mu_i) \mathcal{F}_\gamma(P_+), \quad (3)$$

where the structure function \mathcal{F}_γ depends on the photon energy via $P_+ = M_B - 2E_\gamma$. The prefactor contains the electromagnetic fine-structure constant α normalized at $q^2 = 0$, two powers of the running b -quark mass (defined in the $\overline{\text{MS}}$ scheme) originating from the electromagnetic dipole operator $Q_{7\gamma}$ in the effective weak Hamiltonian, and the square of the corresponding Wilson coefficient $C_{7\gamma}^{\text{eff}}$, which is needed at next-to-leading order in renormalization-group improved perturbation theory [12]. Renormalization-group running from the hard scale $\mu_h \sim m_b$ to the intermediate scale $\mu_i \sim \sqrt{m_b \Lambda_{\text{QCD}}}$ gives rise to the Sudakov factor $U(\mu_h, \mu_i)$, whose explicit form is discussed in Appendix A.1. We keep U and $|C_{7\gamma}^{\text{eff}}|^2$ outside of the structure function; however, it is understood that when combining it with a contribution to \mathcal{F}_γ these perturbative quantities should be expanded for consistency to the required order in perturbation theory.

2.1 Leading-power factorization formula

At leading order in Λ_{QCD}/m_b the structure function \mathcal{F}_γ factorizes as [17]

$$\mathcal{F}_\gamma^{(0)}(P_+) = |H_s(\mu_h)|^2 \int_0^{P_+} d\hat{\omega} m_b J(m_b(P_+ - \hat{\omega}), \mu_i) \hat{S}(\hat{\omega}, \mu_i). \quad (4)$$

At this order a single non-perturbative structure function arises, called the leading shape function [3] and denoted by $\hat{S}(\hat{\omega}, \mu_i)$. It is defined in terms of a non-local matrix element in heavy-quark effective theory (HQET). Renormalization-group running between the intermediate scale and a low hadronic scale is avoided when using the shape functions renormalized at the intermediate scale μ_i . Evolution effects below this scale are universal (i.e., process independent) and so can be absorbed into the renormalized shape function. Short-distance contributions from scales above $\mu_h \sim m_b$ are included in the hard function H , which in practice is obtained by matching the effective weak Hamiltonian onto a current operator in soft-collinear effective theory (SCET). At next-to-leading order in perturbation theory, the result reads

$$\begin{aligned} H_s(\mu_h) = & 1 + \frac{C_F \alpha_s(\mu_h)}{4\pi} \left(-2 \ln^2 \frac{m_b}{\mu_h} + 7 \ln \frac{m_b}{\mu_h} - 6 - \frac{\pi^2}{12} \right) + \varepsilon_{\text{ew}} \\ & + \frac{C_{8g}^{\text{eff}}(\mu_h)}{C_{7\gamma}^{\text{eff}}(\mu_h)} \frac{C_F \alpha_s(\mu_h)}{4\pi} \left(-\frac{8}{3} \ln \frac{m_b}{\mu_h} + \frac{11}{3} - \frac{2\pi^2}{9} + \frac{2\pi i}{3} \right) \\ & + \frac{C_1(\mu_h)}{C_{7\gamma}^{\text{eff}}(\mu_h)} \frac{C_F \alpha_s(\mu_h)}{4\pi} \left(\frac{104}{27} \ln \frac{m_b}{\mu_h} + g(z) - \frac{V_{ub} V_{us}^*}{V_{tb} V_{ts}^*} [g(0) - g(z)] \right) + \varepsilon_{\text{peng}}, \quad (5) \end{aligned}$$

where the variable $z = (m_c/m_b)^2$ denotes the ratio of quark masses relevant to charm-loop penguin diagrams, and the ‘‘penguin function’’ $g(z)$ can be approximated by the first few terms of its Taylor expansion,

$$\begin{aligned}
g(z) = & -\frac{833}{162} - \frac{20\pi i}{27} + \frac{8\pi^2}{9} z^{3/2} \\
& + \frac{2z}{9} [48 - 5\pi^2 - 36\zeta_3 + (30\pi - 2\pi^3)i + (36 - 9\pi^2 + 6\pi i) \ln z + (3 + 6\pi i) \ln^2 z + \ln^3 z] \\
& + \frac{2z^2}{9} [18 + 2\pi^2 - 2\pi^3 i + (12 - 6\pi^2) \ln z + 6\pi i \ln^2 z + \ln^3 z] \\
& + \frac{z^3}{27} [-9 - 14\pi^2 + 112\pi i + (182 - 48\pi i) \ln z - 126 \ln^2 z] + \dots
\end{aligned} \tag{6}$$

The remaining two corrections, $\varepsilon_{\text{ew}} \approx -1.5\%$ and $\varepsilon_{\text{peng}} \approx -0.6\%$, account for small electroweak corrections and the effects of penguin contractions of operators other than $Q_1^{u,c}$, respectively. The differential decay rate (3) is formally independent of the matching scales μ_h and μ_i . The dependence on the hard scale in the Sudakov factor is canceled by the hard function, and the μ_i dependence compensates the scale dependence of the convolution integral $J(\mu_i) \otimes \hat{S}(\mu_i)$.

Finally let us discuss the jet function J , which appears as the hard-scattering kernel in the convolution integral in (4). It can be written in terms of distributions that act on the shape function \hat{S} . At one-loop level, it is given by [6, 7]

$$J(p^2, \mu) = \delta(p^2) \left[1 + \frac{C_F \alpha_s(\mu)}{4\pi} (7 - \pi^2) \right] + \frac{C_F \alpha_s(\mu)}{4\pi} \left[\frac{1}{p^2} \left(4 \ln \frac{p^2}{\mu^2} - 3 \right) \right]_*^{[\mu^2]}, \tag{7}$$

where the star distributions have the following effect on a function f when integrated over a domain Q^2 [13]:

$$\begin{aligned}
\int_{\leq 0}^{Q^2} dp^2 \left[\frac{1}{p^2} \right]_*^{[\mu^2]} f(p^2) &= \int_0^{Q^2} dp^2 \frac{f(p^2) - f(0)}{p^2} + f(0) \ln \frac{Q^2}{\mu^2}, \\
\int_{\leq 0}^{Q^2} dp^2 \left[\frac{1}{p^2} \ln \frac{p^2}{\mu^2} \right]_*^{[\mu^2]} f(p^2) &= \int_0^{Q^2} dp^2 \frac{f(p^2) - f(0)}{p^2} \ln \frac{p^2}{\mu^2} + \frac{1}{2} f(0) \ln^2 \frac{Q^2}{\mu^2}.
\end{aligned} \tag{8}$$

2.2 Kinematical power corrections

There exists a class of power corrections to (4) that do not involve new hadronic quantities. Instead, the power suppression results from the restriction of certain variables (P_+ in the present case) to a region where they are kinematically suppressed (here $P_+ \ll M_B$). These terms are associated with the leading-order shape function. Technically, these ‘‘kinematic’’ power corrections arise in the matching of QCD correlators onto higher-dimensional SCET and HQET operators. The corresponding terms are known in fixed-order perturbation theory, without scale separation and renormalization-group resummation [14, 15] (see also [16]). To perform a complete RG analysis of even the first-order terms in $1/m_b$ is beyond the scope

of the present work. Since, as we will see later, power corrections only account for small corrections to the decay rates, an approximate treatment will suffice. To motivate it, we note the following two facts [17]: First, while the anomalous dimensions of the relevant subleading SCET and HQET operators are only known for a few cases [18], the leading Sudakov double logarithms are the same as for the terms of leading power, because they have a geometric origin in terms of Wilson lines [19]. The leading Sudakov double logarithms are therefore the same as those resummed into the function U in (3). Secondly, the kinematical power corrections in $\bar{B} \rightarrow X_s \gamma$ decay are associated with gluon emission into the hadronic final state X_s . Because of the kinematical restriction to low-mass final states, i.e. $M_X^2 \sim M_B \Lambda_{\text{QCD}}$, we associate a coupling $\alpha_s(\bar{\mu})$ with these terms, where typically $\bar{\mu} \sim \mu_i$. Strictly speaking, however, the scale ambiguity associated with the choice of $\bar{\mu}$ could only be resolved by computing the relevant anomalous dimensions.

Within this approximation, the kinematical power corrections to the structure function \mathcal{F}_γ can be extracted from [16, 17]. We find it convenient to express the result in terms of the variable

$$x = \frac{P_+ - \hat{\omega}}{M_B - P_+}, \quad (9)$$

which in the shape-function region scales like Λ_{QCD}/m_b . We obtain

$$\begin{aligned} \mathcal{F}_\gamma^{\text{kin}}(P_+) &= \frac{1}{M_B - P_+} \frac{C_F \alpha_s(\bar{\mu})}{4\pi} \sum_{\substack{i,j=1,7,8 \\ i \leq j}} \frac{C_i(\mu_h) C_j(\mu_h)}{C_{7\gamma}^{\text{eff}}(\mu_h)^2} \int_0^{P_+} d\hat{\omega} \hat{S}(\hat{\omega}, \mu_i) h_{ij}(x) \\ &\quad - \frac{\lambda_2}{9m_c^2} \frac{C_1(\mu_h)}{C_{7\gamma}^{\text{eff}}(\mu_h)} \hat{S}(P_+, \mu_i). \end{aligned} \quad (10)$$

The coefficient functions $h_{ij}(x)$ are

$$\begin{aligned} h_{77}(x) &= -3(5 + 2x) + 2(8 + 9x + 3x^2) \ln \left(1 + \frac{1}{x} \right), \\ h_{88}(x) &= \frac{2}{9} (1 + 3x + 4x^2 + 2x^3) \left[2 \ln \frac{m_b}{m_s} - \ln \left(1 + \frac{1}{x} \right) \right] - \frac{1}{9} (3 + 9x + 16x^2 + 8x^3), \\ h_{78}(x) &= \frac{2}{3} (5 + 8x + 4x^2) - \frac{8}{3} x(1+x)^2 \ln \left(1 + \frac{1}{x} \right), \\ h_{11}(x) &= \frac{16}{9} \int_0^1 du (1+x-u) \left| \frac{z(1+x)}{u} G \left(\frac{u}{z(1+x)} \right) + \frac{1}{2} \right|^2, \\ h_{17}(y) &= -3h_{18}(y) = -\frac{8}{3} \int_0^1 du u \operatorname{Re} \left[\frac{z(1+x)}{u} G \left(\frac{u}{z(1+x)} \right) + \frac{1}{2} \right], \end{aligned} \quad (11)$$

where as before $z = (m_c/m_b)^2$, and

$$G(t) = \begin{cases} -2 \arctan^2 \sqrt{t/(4-t)} & ; t < 4, \\ 2 \left(\ln \left[(\sqrt{t} + \sqrt{t-4})/2 \right] - \frac{i\pi}{2} \right)^2 & ; t \geq 4. \end{cases} \quad (12)$$

In the shape-function region, the expressions for $h_{ij}(x)$ could, if desired, be expanded in a power series in $x = O(\Lambda_{\text{QCD}}/m_b)$, and this would generate a series of power-suppressed terms $\mathcal{F}_\gamma^{\text{kin}(n)}(P_+)$ with $n \geq 1$, where the superscript “n” indicates the order in the $1/m_b$ expansion. Note that this expansion would contain single logarithms $\ln x \sim \ln(\Lambda_{\text{QCD}}/m_b)$. These are precisely the logarithms that would be resummed in a more proper treatment using effective field-theory methods.

Outside the shape-function region the variable x can take on arbitrarily large positive values, and $\mathcal{F}_\gamma^{\text{kin}}(P_+)$ is no longer power suppressed. Note for $P_+ \rightarrow M_B$ (corresponding to $x \rightarrow \infty$ and $E_\gamma \rightarrow 0$), most functions $h_{ij}(x)$ grow like x^2 or weaker, so that the spectrum tends to a constant. The only (well known) exception is $h_{88}(x)$, which grows like x^3 , giving rise to a $1/E_\gamma$ soft-photon singularity.

The main effect of the kinematical power corrections (10) to the photon spectrum is the appearance of a radiative tail extending into the region of smaller photon energies. They therefore become more and more significant as the domain of integration over E_γ is increased.

2.3 Subleading shape-function contributions

At Λ_{QCD}/m_b in power counting, different combinations of subleading shape functions enter the $\bar{B} \rightarrow X_s \gamma$ and $\bar{B} \rightarrow X_u l^- \bar{\nu}$ decay distributions [20, 21, 22, 23]. They provide the dominant “hadronic” power correction, which must be combined with the “kinematic” power corrections discussed in the previous section. We include their effects using the results of recent calculations in [11, 24, 25]. We use the notation of [11] for consistency. Little is known about these structure functions apart from expressions for their first few moments. In particular, the norms of these functions vanish at tree level, while their first moments are determined by the HQET parameters λ_1 and λ_2 , which are defined via the forward B -meson matrix elements of the kinetic-energy and the chromo-magnetic operators, respectively [26].

For the case of $\bar{B} \rightarrow X_s \gamma$ decay, subleading shape-function contributions are currently only known for the matrix elements of the dipole operator $Q_{7\gamma}$, and the corresponding hard and jet functions have been computed at tree level. (At this order, a δ -distribution identifies $\hat{\omega}$ with P_+ .) Adopting the notations of [11], the relevant subleading shape functions are $\hat{t}(\hat{\omega})$, $\hat{u}(\hat{\omega})$, and $\hat{v}(\hat{\omega})$. An additional function, called s , has been absorbed by a redefinition of the leading shape function, and it is included in our definition of $\hat{S}(\hat{\omega})$. Roughly speaking, $\hat{u}(\hat{\omega})$ is the “light-cone generalization” of the local HQET kinetic-energy operator. The functions $\hat{v}(\hat{\omega})$ and $\hat{t}(\hat{\omega})$ are both generalizations of the local chromo-magnetic HQET operator, but $\hat{t}(\hat{\omega})$ contains also a light-cone chromo-electric operator, which has no equivalent in the local OPE expansion. (Such a contribution arises since in the SCET expansion we have two external 4-vectors, n and v , while in the HQET expansion we have only v .) We can then write down the contribution to the photon spectrum as

$$\mathcal{F}_\gamma^{\text{had}(1)}(P_+) = \frac{1}{M_B - P_+} \left[-(\bar{\Lambda} - P_+) \hat{S}(P_+) - \hat{t}(P_+) + \hat{u}(P_+) - \hat{v}(P_+) \right]. \quad (13)$$

Compared to [11], we have replaced one power of $1/m_b$ with $1/(M_B - P_+)$, which is exact at this order. (The support of the shape functions restricts P_+ to be of order Λ_{QCD} .) The appearance

of the parameter $\bar{\Lambda} = M_B - m_b$ is peculiar to the subleading shape-function contributions. This quantity is defined via the first moment of the leading-order shape function.

The formula given above can be modified to suit the purpose of extracting the shape function from the photon spectrum better. To this end, we absorb a linear combination of the subleading shape functions into a redefinition of the leading shape function, but in such a way that the moment relations for the leading structure function remain unchanged to the order we are working. This is accomplished by defining

$$\mathcal{S}(\hat{\omega}) \equiv \hat{S}(\hat{\omega}) + \frac{2(\bar{\Lambda} - \hat{\omega}) \hat{S}(\hat{\omega}) - \hat{t}(\hat{\omega}) + \hat{u}(\hat{\omega}) - \hat{v}(\hat{\omega})}{M_B - \hat{\omega}}. \quad (14)$$

When using \mathcal{S} instead of \hat{S} in the leading-power formula (4), the subleading shape-function contribution becomes

$$\mathcal{F}_\gamma^{\text{had}(1)}(P_+) = -\frac{3(\bar{\Lambda} - P_+)}{M_B - P_+} \mathcal{S}(P_+, \mu_i). \quad (15)$$

This replacement will also influence the result at order $1/m_b^2$ presented in the following section.

2.4 Residual hadronic power corrections

At order $1/m_b^2$ a new set of sub-subleading shape functions enter, which so far have not been studied in the literature. Since the functional form of even the subleading shape functions (at order $1/m_b$) is rather uncertain, there is no need to worry too much about the precise form of sub-subleading shape functions. Most of their effects can be absorbed into the sub-leading functions. An exception, however, are terms that survive when the sub-subleading shape functions are integrated over a wide domain. Whereas the norms of all subleading ($\sim 1/m_b$) shape functions vanish, the norms of the sub-subleading shape functions ($\sim 1/m_b^2$) are in general non-zero and given in terms of the heavy-quark parameters λ_1 and λ_2 . Our strategy will thus be as follows: We start from the well-known expressions for the (tree-level) second-order power corrections to the $\bar{B} \rightarrow X_s \gamma$ photon spectrum [29] (and similarly for the triple-differential $\bar{B} \rightarrow X_u l^- \bar{\nu}$ decay distribution [8, 9], see Section 3.4). They are of the form λ_i/m_b^2 times one of the singular distributions $\delta(p^2)$, $\delta'(p^2)$, or $\delta''(p^2)$, where $p^2 = (m_b v - q)^2$ is the invariant partonic mass squared of the final-state jet. As mentioned earlier, the power counting in the shape-function region is different from the one used in OPE calculations, and indeed a good portion of these OPE $1/m_b^2$ terms is already accounted for by the contributions proportional to the leading and sub-leading shape functions in (4) and (13) or (15), respectively. We identify the corresponding terms using the moment relations for the shape functions derived in [3] and [20] (see also [11]). In particular, this accounts for all terms at order $1/m_b^2$ in the OPE which contain derivatives of $\delta(p^2)$. We account for the remaining terms of the form $\lambda_i/m_b^2 \delta(p^2)$ by replacing

$$\begin{aligned} \delta(p^2) &= \delta(p_+ p_-) = \frac{1}{p_- - p_+} \int d\omega \delta(p_+ - \omega) \delta(\omega) \\ &\rightarrow \frac{1}{P_- - P_+} \int d\hat{\omega} \delta(P_+ - \hat{\omega}) \hat{S}(\hat{\omega}) = \frac{\hat{S}(P_+)}{P_- - P_+}. \end{aligned} \quad (16)$$

Here p_{\pm} are the light-cone projections of the partonic momentum p^{μ} , which are related to the hadronic quantities P_{\pm} by $P_{\pm} = p_{\pm} + \bar{\Lambda}$. Similarly, $\hat{\omega} = \bar{\Lambda} - \omega$.

The result of these manipulations is

$$\mathcal{F}_{\gamma}^{\text{had}(2)} = \frac{1}{(M_B - P_+)^2} \left(\frac{\lambda_1 - 3\lambda_2}{2} \right) \hat{\mathcal{S}}(P_+, \mu_i). \quad (17)$$

Together with (4) and (13), this accounts for all known first- and second-order power corrections to the $\bar{B} \rightarrow X_s \gamma$ photon spectrum, both in the shape-function region and in the OPE region. As mentioned earlier, however, the redefinition (14) of the leading shape function from $\hat{\mathcal{S}}$ to \mathcal{S} affects the form of the second-order power corrections. When (15) is used instead of (13), as we intend to do, then the above expression changes to

$$\mathcal{F}_{\gamma}^{\text{had}(2)} = \frac{1}{(M_B - P_+)^2} \left(-\frac{\lambda_1 + 9\lambda_2}{2} \right) \mathcal{S}(P_+, \mu_i). \quad (18)$$

The hadronic parameter λ_2 determines the leading contribution to the hyperfine splitting between the masses of B and B^* mesons through $m_{B^*}^2 - m_B^2 = 4\lambda^2 + O(1/m_b)$ [26], from which it follows that $\lambda_2 \approx 0.12 \text{ GeV}^2$. The value of the parameter λ_1 is more uncertain. In much the same way as the b -quark pole mass it is affected by infrared renormalon ambiguities [27, 28], and it is therefore better to eliminate λ_1 in favor of some observable. To this end, we will later replace $\lambda_1 \rightarrow -\mu_{\pi}^2$, where μ_{π}^2 is related to the width of the renormalized leading-order shape function.

In Section 5 we study the numerical impact of second-order power corrections on various $\bar{B} \rightarrow X_u l^- \bar{\nu}$ partial rates and find their effects to be tiny. It is therefore a safe approximation to neglect hadronic power corrections of order $1/m_b^3$ or higher. The only possible exception to this conclusion relates to so-called weak annihilation terms in $\bar{B} \rightarrow X_u l^- \bar{\nu}$ decay, which will be included in our error analysis.

3 Inclusive semi-leptonic decays

All hadronic physics in $\bar{B} \rightarrow X_u l^- \bar{\nu}$ decays is encoded in the hadronic tensor $W^{\mu\nu}$, which is defined via the discontinuity of the forward B -meson matrix element of a correlator of two flavor-changing weak currents $J^{\mu} = \bar{u} \gamma^{\mu} (1 - \gamma_5) b$. Explicitly it is

$$W^{\mu\nu} = \frac{1}{2M_B} \frac{1}{\pi} \text{Im} \langle \bar{B}(v) | i \int d^4x e^{iq \cdot x} \text{T} \{ J^{\dagger\mu}(0), J^{\nu}(x) \} | \bar{B}(v) \rangle, \quad (19)$$

where v is the B -meson velocity, and q the momentum carried by the lepton pair. The hadronic tensor decomposes into five structure functions W_i , which are the coefficients of the five possible Lorentz structures built out of two independent 4-vectors. Typical choices for these two vectors are q and v , p and v , etc. Here, as above, $p = m_b v - q$ is the momentum of the jet of light particles into which the b quark decays. In principle, all choices are equivalent, and it is solely a matter of convenience which basis one picks.

The triple differential decay rate can then be expressed in terms of kinematical prefactors and the functions W_i . It is a known fact that the total decay rate is proportional to five

powers of the b -quark mass. Further sensitivity to m_b is picked up for partial decay rates by the kinematical cuts. For example, cutting on the leptonic invariant mass $q^2 > q_0^2$ introduces roughly five additional powers, and the resulting partial decay rate is proportional to $(m_b)^a$ with $a \approx 10$ [30, 31]. This is the reason why theoretical predictions were typically made for event fractions, so that at least the five powers of the total rate drop out. For practical purposes, however, this procedure presents no advantage as the value of the total decay rate cannot be measured. Furthermore, the m_b dependence of the total rate is clearly related to the m_b dependence of partial rates, and it is important to take this correlation into account when calculating event fractions. In Section 5, where we present theoretical predictions, we will thus focus directly on predictions of partial decay rates, not event fractions. The question at hand is how information about m_b enters the triple differential decay rate. Potentially there are two sources, the hadronic structure functions W_i and their kinematical prefactors. Whether or not m_b appears explicitly in the prefactors depends on the decomposition of $W^{\mu\nu}$, i.e. the choice of vectors used to form the five possible Lorentz structures.

A very useful set of 4-vectors turns out to be (v, n) , where n is a light-like vector in the spatial direction of the jet of light particles. In SCET, n denotes the collinear light-cone direction of the particles in the jet, which is typically set to be along the z -axis. The normalization is chosen such that $v \cdot n = 1$, so that $n^\mu = (1, 0, 0, 1)$ in the rest frame of the B meson. The conjugate direction to n is denoted by $\bar{n}^\mu = (1, 0, 0, -1)$ and marks the collinear direction of the photon in $\bar{B} \rightarrow X_s \gamma$ decays, or the collinear light-cone direction of the lepton pair in $\bar{B} \rightarrow X_u l^- \bar{\nu}$ decays. We then decompose

$$W^{\mu\nu} = (n^\mu v^\nu + n^\nu v^\mu - g^{\mu\nu} - i\epsilon^{\mu\nu\alpha\beta} n_\alpha v_\beta) \tilde{W}_1 - g^{\mu\nu} \tilde{W}_2 + v^\mu v^\nu \tilde{W}_3 + (n^\mu v^\nu + n^\nu v^\mu) \tilde{W}_4 + n^\mu n^\nu \tilde{W}_5. \quad (20)$$

The structure functions \tilde{W}_i all have mass dimension -1 in this basis. In terms of the \tilde{W}_i functions the triple differential decay rate reads

$$\frac{d^3\Gamma_u}{dP_+ dP_- dP_l} = \frac{G_F^2 |V_{ub}|^2}{16\pi^3} U_y(\mu_h, \mu_i) (M_B - P_+) \left[(P_- - P_l)(M_B - P_- + P_l - P_+) \mathcal{F}_1 + (M_B - P_-)(P_- - P_+) \mathcal{F}_2 + (P_- - P_l)(P_l - P_+) \mathcal{F}_3 \right], \quad (21)$$

where we have collected the relevant combinations of \tilde{W}_i into the three functions

$$U_y(\mu_h, \mu_i) \mathcal{F}_1 = \tilde{W}_1, \quad U_y(\mu_h, \mu_i) \mathcal{F}_2 = \frac{\tilde{W}_2}{2}, \quad U_y(\mu_h, \mu_i) \mathcal{F}_3 = \left(\frac{y}{4} \tilde{W}_3 + \tilde{W}_4 + \frac{1}{y} \tilde{W}_5 \right), \quad (22)$$

and defined a new kinematical variable

$$y = \frac{P_- - P_+}{M_B - P_+}; \quad 0 \leq y \leq 1. \quad (23)$$

The leading Sudakov factor $U_y(\mu_h, \mu_i)$ has been factored out in (21) for convenience, as we have done earlier in (3). The function $U_y(\mu_h, \mu_i)$ differs from the corresponding function in $\bar{B} \rightarrow X_s \gamma$ decay by a y -dependent factor,

$$U_y(\mu_h, \mu_i) = U(\mu_h, \mu_i) y^{-2a_\Gamma(\mu_h, \mu_i)}, \quad (24)$$

where the function a_Γ in the exponent is related to the cusp anomalous dimension and is given in Appendix A.2.

Eq. (21) for the triple differential rate is exact. Note that there is no reference to the b -quark mass at this point. The only dependence on m_b is through the structure functions $\mathcal{F}_i(P_+, y)$ (via hard matching corrections and via the moment constraints on the shape function \hat{S}), which are independent of the leptonic variable P_l . The fact that the total decay rate Γ_u is proportional to m_b^5 is not in contradiction with (21). It is instructive to demonstrate how these five powers of m_b are recovered in our approach. At tree level and leading power the functions \mathcal{F}_2 and \mathcal{F}_3 vanish, while $\mathcal{F}_1 = \hat{S}(P_+)$. Integrating over the full range of P_l and P_- builds up five powers of $(M_B - P_+)$. For the purpose of illustration, let us rename² the P_+ variable to $\hat{\omega}$ in the last integration, so that the total decay rate is given as

$$\begin{aligned} \Gamma_u &= \frac{G_F^2 |V_{ub}|^2}{192\pi^3} \int_0^{M_B} d\hat{\omega} (M_B - \hat{\omega})^5 \hat{S}(\hat{\omega}) = \frac{G_F^2 |V_{ub}|^2}{192\pi^3} \int_{-m_b}^{\bar{\Lambda}} d\omega (m_b + \omega)^5 S(\omega) \\ &= \frac{G_F^2 |V_{ub}|^2}{192\pi^3} (m_b + \langle\omega\rangle)^5 \left[1 + O\left(\frac{1}{m_b^2}\right) \right]. \end{aligned} \quad (25)$$

At tree level, the first moment of the shape function $S(\omega)$ vanishes. Beyond tree level this is no longer the case, and the average $\langle\omega\rangle$ depends on the size of the integration domain. The above observation motivates the use of the shape-function scheme [7], in which the b -quark mass is defined as $m_b^{\text{SF}} = m_b^{\text{pole}} + \langle\omega\rangle$. After this is done, (25) recovers the form of the conventional OPE result.

Eq. (21) and the above argument tell us that the differential rate is a priori rather insensitive to the b -quark mass in the endpoint region, where P_+ (and therefore $\langle\hat{\omega}\rangle$) is a small quantity. Only when the rates are integrated over a sufficiently wide domain, so that shape-function integrals can be approximated using a moment expansion, a dependence on m_b enters indirectly via the first moment of the leading-order shape functions. Likewise, a dependence on other HQET parameters such as λ_1 enters via the sensitivity to higher moments.

In the remainder of this section we present the various contributions to the structure functions \mathcal{F}_i , following the same line of presentation as we did in the case of $\bar{B} \rightarrow X_s \gamma$ decay in Section 2. As before, while the the resulting expressions are “optimized” for the shape-function region, they can be used over the entire phase space and give the correct result for the total decay rate up to corrections of $O(\alpha_s^2)$. In the shape-function region, where P_+ is a small quantity, one may organize \mathcal{F}_i as a series in inverse powers of $1/(M_B - P_+)$. No assumption about the variable y is made, which is treated as an $O(1)$ quantity.³ A preview of the results of our calculation is depicted in Figure 1, which shows the hadronic phase space and an illustration of our prediction of the distribution of events in the plane (P_+, P_-) .

²More precisely, we interchange the order of integration of $\int dP_+ \int d\hat{\omega} (M_B - P_+)^5 \delta(P_+ - \hat{\omega}) \hat{S}(\hat{\omega})$ and leave the $\hat{\omega}$ integration for last. The $\delta(P_+ - \hat{\omega})$ is the tree-level jet function.

³In the shape-function region, where $P_+ \ll P_-$, we have $y \approx p_-/m_b$, which is the variable used in the leading-power analysis in [7].

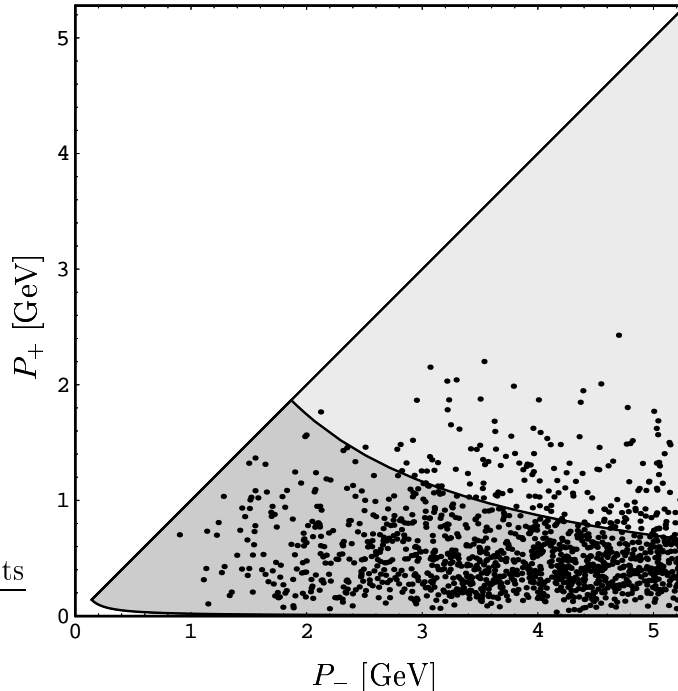


Figure 1: The hadronic phase space in P_+ and P_- . Each point represents an event in a Monte-Carlo simulation using the results of this paper. While the shape-function region of large P_- and small P_+ is highly populated, there is not a single event with P_+ larger than 3 GeV out of the 1300 events generated.

3.1 Leading-power factorization formula

The leading-power expressions for the hadronic structure functions W_i have been calculated in [7] at one-loop order in renormalization-group improved perturbation theory. At this level, \mathcal{F}_2 does not obtain a contribution, whereas \mathcal{F}_1 and \mathcal{F}_3 do. Symbolically, they have been factorized as $H J \otimes \hat{S}$, i.e., into a hard function H and the convolution of a jet function J and the leading shape function \hat{S} . More precisely,

$$\begin{aligned}\mathcal{F}_1^{(0)}(P_+, y) &= H_u(y, \mu_h) \int_0^{P_+} d\hat{\omega} y m_b J(y m_b (P_+ - \hat{\omega}), \mu_i) \hat{S}(\hat{\omega}, \mu_i), \\ \mathcal{F}_3^{(0)}(P_+, y) &= \frac{C_F \alpha_s(\mu_h)}{4\pi} \frac{2 \ln y}{1-y} \hat{S}(P_+, \mu_i).\end{aligned}\tag{26}$$

The hard function H_u in \mathcal{F}_1 is given by

$$H_u(y, \mu_h) = 1 + \frac{C_F \alpha_s(\mu_h)}{4\pi} \left[-4 \ln^2 \frac{y m_b}{\mu_h} + 10 \ln \frac{y m_b}{\mu_h} - 4 \ln y - \frac{2 \ln y}{1-y} - 4 L_2(1-y) - \frac{\pi^2}{6} - 12 \right].\tag{27}$$

As before, the result is independent of the matching scales $\mu_h \sim m_b$ and $\mu_i \sim \sqrt{m_b \Lambda_{\text{QCD}}}$. The jet function J has already been given in (7). Note that the b -quark mass appears only as the argument of logarithms, where it is needed to set the renormalization scales.

3.2 Kinematical power corrections

As in the case of $\bar{B} \rightarrow X_s \gamma$ decay, there is a class of power corrections to the $\bar{B} \rightarrow X_u l^- \bar{\nu}$ decay distributions which are small only because of the restriction to certain regions in phase space, but which are not associated with new hadronic parameters. In the present case, these terms can be extracted from the one-loop expressions derived in [13]. They are then convoluted with the leading shape function. As previously, the scale separation that can be achieved for these power-suppressed terms is only approximate, and we thus assign a coupling $\alpha_s(\bar{\mu})$ with them, where the scale $\bar{\mu}$ is expected to be of order $\mu_i \sim \sqrt{m_b \Lambda_{\text{QCD}}}$ but is strictly not determined at this order.

The resulting expressions for the structure functions can be written in a compact form in terms of the variables x and y defined in (9) and (23). We find

$$\begin{aligned}
\mathcal{F}_1^{\text{kin}}(P_+, y) &= \frac{1}{M_B - P_+} \frac{C_F \alpha_s(\bar{\mu})}{4\pi} \int_0^{P_+} d\hat{\omega} \hat{S}(\hat{\omega}, \mu_i) \\
&\quad \times \left[\frac{f_1(x, y)}{(1+x)^2 y(x+y)} - \frac{2 g_1(x, y)}{x(1+x)^2 y^2(x+y)} \ln\left(1 + \frac{y}{x}\right) - \frac{4}{x} \ln\left(y + \frac{y}{x}\right) \right], \\
\mathcal{F}_2^{\text{kin}}(P_+, y) &= \frac{1}{M_B - P_+} \frac{C_F \alpha_s(\bar{\mu})}{4\pi} \int_0^{P_+} d\hat{\omega} \hat{S}(\hat{\omega}, \mu_i) \\
&\quad \times \left[\frac{f_2(x, y)}{(1+x)^2 y^2(x+y)} - \frac{2x g_2(x, y)}{(1+x)^2 y^3(x+y)} \ln\left(1 + \frac{y}{x}\right) \right], \\
\mathcal{F}_3^{\text{kin}}(P_+, y) &= \frac{1}{M_B - P_+} \frac{C_F \alpha_s(\bar{\mu})}{4\pi} \int_0^{P_+} d\hat{\omega} \hat{S}(\hat{\omega}, \mu_i) \\
&\quad \times \left[\frac{f_3(x, y)}{(1+x)^2 y^3(x+y)} + \frac{2 g_3(x, y)}{(1+x)^2 y^4(x+y)} \ln\left(1 + \frac{y}{x}\right) \right], \tag{28}
\end{aligned}$$

where the functions f_i, g_i are given by

$$\begin{aligned}
f_1(x, y) &= -9y + 10y^2 + x(-16 + 12y + 6y^2) + x^2(13y - 12), \\
g_1(x, y) &= -2y^3 - 2xy^2(4 + y) - x^2y(12 + 4y + y^2) - 4x^3(y + 2) + 3x^4(y - 2), \\
f_2(x, y) &= y^2 + xy(8 + 4y + y^2) + 3x^2y(10 + y) + x^3(12 + 19y) + 10x^4, \\
g_2(x, y) &= 2y^2 + 4xy(1 + 2y) + x^2y(18 + 5y) + 6x^3(1 + 2y) + 5x^4, \\
f_3(x, y) &= 2y^3(2y - 11) + xy^2(-94 + 29y + 2y^2) + 2x^2y(-72 + 18y + 13y^2) \\
&\quad + x^3(-72 - 42y + 70y^2 - 3y^3) - 10x^4(6 - 6y + y^2), \\
g_3(x, y) &= 4y^4 - 6x(y - 5)y^3 - 4x^2y^2(-20 + 6y + y^2) + x^3y(90 - 10y - 28y^2 + y^3) \\
&\quad + x^4(36 + 36y - 50y^2 + 4y^3) + 5x^5(6 - 6y + y^2). \tag{29}
\end{aligned}$$

The above formulae are the exact $O(\alpha_s)$ corrections to the leading-power expression. This means that they will give rise to the correct result for the total rate up to that order, when

integrating over the entire phase space. In the shape-function region $P_+ \ll P_-$ they can be expanded in terms of $1/m_b$, if desired. To this end, we count $y = O(1)$ and $x = O(1/m_b)$, and expand the functions f_i, g_i in a power series in x . Note that this organizes the $1/m_b$ expansion as an expansion in powers of the hadronic variable $1/(M_B - P_+)$. The leading terms in this expansion read

$$\begin{aligned}
\mathcal{F}_1^{\text{kin}(1)}(P_+, y) &= \frac{1}{M_B - P_+} \frac{C_F \alpha_s(\bar{\mu})}{4\pi} \int_0^{P_+} d\hat{\omega} \hat{S}(\hat{\omega}, \mu_i) \left[6 - \frac{5}{y} + \left(\frac{12}{y} - 4 \right) \ln \frac{y}{x} \right], \\
\mathcal{F}_2^{\text{kin}(1)}(P_+, y) &= \frac{1}{M_B - P_+} \frac{C_F \alpha_s(\bar{\mu})}{4\pi} \int_0^{P_+} d\hat{\omega} \hat{S}(\hat{\omega}, \mu_i) \left[\frac{1}{y} \right], \\
\mathcal{F}_3^{\text{kin}(1)}(P_+, y) &= \frac{1}{M_B - P_+} \frac{C_F \alpha_s(\bar{\mu})}{4\pi} 2 \int_0^{P_+} d\hat{\omega} \hat{S}(\hat{\omega}, \mu_i) \left[2 - \frac{11}{y} + \frac{4}{y} \ln \frac{y}{x} \right]. \tag{30}
\end{aligned}$$

Further accuracy can be achieved by adding the next-order corrections, for which we obtain

$$\begin{aligned}
\mathcal{F}_1^{\text{kin}(2)}(P_+, y) &= \frac{1}{(M_B - P_+)^2} \frac{C_F \alpha_s(\bar{\mu})}{4\pi} \int_0^{P_+} d\hat{\omega} (P_+ - \hat{\omega}) \hat{S}(\hat{\omega}, \mu_i) \\
&\quad \times \left[\frac{3}{y^2} + \frac{16}{y} - 12 + 2 \left(\frac{6}{y^2} - \frac{10}{y} + 3 \right) \ln \frac{y}{x} \right], \\
\mathcal{F}_2^{\text{kin}(2)}(P_+, y) &= \frac{1}{(M_B - P_+)^2} \frac{C_F \alpha_s(\bar{\mu})}{4\pi} \int_0^{P_+} d\hat{\omega} (P_+ - \hat{\omega}) \hat{S}(\hat{\omega}, \mu_i) \\
&\quad \times \left[1 + \frac{2}{y} + \frac{7}{y^2} - \frac{4}{y^2} \ln \frac{y}{x} \right], \\
\mathcal{F}_3^{\text{kin}(2)}(P_+, y) &= \frac{1}{(M_B - P_+)^2} \frac{C_F \alpha_s(\bar{\mu})}{4\pi} 2 \int_0^{P_+} d\hat{\omega} (P_+ - \hat{\omega}) \hat{S}(\hat{\omega}, \mu_i) \\
&\quad \times \left[-3 + \frac{69}{2y} - \frac{32}{y^2} + \left(\frac{26}{y^2} - \frac{14}{y} \right) \ln \frac{y}{x} \right]. \tag{31}
\end{aligned}$$

In the various regions of phase space of interest to the determination of $|V_{ub}|$, the above terms (30) and (31) approximate the full result (28) very well (see Section 5 below).

Let us comment here on a technical point already mentioned in the Introduction. When combined with the phase-space factors in (21), the exact expressions for $\mathcal{F}_i^{\text{kin}}$ in (28) are regular in the limit $P_- \rightarrow P_+$, corresponding to $y \rightarrow 0$. However, this feature is not automatically ensured when the structure functions, but not the phase-space factors, are expanded about the heavy-quark limit. With our choice of the variables x and y , we encounter terms as singular as $1/y^n$ at n -th order in the expansion, as is obvious from the explicit expressions above. Phase space scales like y^2 in the limit $y \rightarrow 0$ (note that $P_l \rightarrow P_+$ as $P_- \rightarrow P_+$ because of (2)), so that the results (30) and (31) can be applied without encountering any kinematical singularities. In order to achieve this, it was crucial to define the variable y in the way we did in (23). We emphasize this point because straightforward application of the technology of SCET and HQET developed in [11, 24, 25] would give an expansion of the structure functions \mathcal{F}_i in powers

of $1/p_-$, whereas phase space is proportional to $4\bar{p}^2 = (p_- - p_+)^2 \propto y^2$. In the kinematical region where $p_+ < 0$, which is allowed due to off-shell binding effects in the B meson, this leads to singularities as $p_- \rightarrow 0$. In order to avoid these singularities, we reorganize the SCET expansion by replacing $1/p_- \rightarrow 1/(p_- - p_+)$, where $|p_+| \ll p_-$ in the shape-function region.

3.3 Subleading shape-function contributions

The contributions from subleading shape functions to arbitrary $\bar{B} \rightarrow X_u l^- \bar{\nu}$ decay distributions have been derived (at tree level) in [24, 11, 25]. The result involves the same set of subleading shape functions as previously discussed in Section 2.3. Again, the structure function \mathcal{F}_2 does not obtain a contribution, while

$$\begin{aligned}\mathcal{F}_1^{\text{hadr}(1)}(P_+, y) &= \frac{1}{M_B - P_+} \left[(\bar{\Lambda} - P_+) \hat{S}(P_+) + \hat{t}(P_+) + \frac{\hat{u}(P_+) - \hat{v}(P_+)}{y} \right], \\ \mathcal{F}_3^{\text{hadr}(1)}(P_+, y) &= \frac{1}{M_B - P_+} \frac{2}{y} \left[-(\bar{\Lambda} - P_+) \hat{S}(P_+) - 2\hat{t}(P_+) + \frac{\hat{t}(P_+) + \hat{v}(P_+)}{y} \right].\end{aligned}\quad (32)$$

At this point we catch up on the discussion from the previous section on $\bar{B} \rightarrow X_s \gamma$. After all, the photon spectrum should be used to fit the function \mathcal{S} of equation (14), which is defined to be a linear combination of the leading shape function \hat{S} and the subleading shape functions $\hat{t}, \hat{u}, \hat{v}$. Since they are the same at leading power, nothing changes in $\mathcal{F}_i^{(0)}$ (except for the simple replacement $\hat{S} \rightarrow \mathcal{S}$, which we from now on assume). At the level of subleading shape functions, $\mathcal{F}_2^{\text{hadr}(1)} = 0$ and $\mathcal{F}_3^{\text{hadr}(1)}$ remain unchanged, while

$$\mathcal{F}_1^{\text{hadr}(1)}(P_+, y) = \frac{1}{M_B - P_+} \left[-(\bar{\Lambda} - P_+) \mathcal{S}(P_+) + 2\hat{t}(P_+) + [\hat{u}(P_+) - \hat{v}(P_+)] \left(\frac{1}{y} - 1 \right) \right]. \quad (33)$$

This means that there resides a linear combination of subleading shape functions in the triple differential decay rate that cannot be extracted from information on the photon spectrum in $\bar{B} \rightarrow X_s \gamma$ decays. In the end, this dependence gives rise to a theoretical uncertainty.

3.4 Residual hadronic power corrections

In analogy with our treatment for the case of $\bar{B} \rightarrow X_s \gamma$ decay, we start from the expressions for the $1/m_b^2$ corrections to the triple differential $\bar{B} \rightarrow X_u l^- \bar{\nu}$ decay rate obtained by applying the OPE to the hadronic tensor [8, 9]. Converting these result into the (n, v) basis and also changing variables from $v \cdot q$ and q^2 to $p_+ = n \cdot p$ and $p_- = \bar{n} \cdot p$, we find

$$\begin{aligned}\tilde{W}_1^{(2)} &= \delta(p_+) \left(1 + \frac{2\lambda_1 - 3\lambda_2}{3p_-^2} \right) + \delta'(p_+) \left(\frac{2\lambda_1 - 3\lambda_2}{3p_-} - \frac{5\lambda_1 + 15\lambda_2}{6m_b} \right) - \delta''(p_+) \frac{\lambda_1}{6}, \\ \tilde{W}_2^{(2)} &= \delta(p_+) \left(\frac{6\lambda_2 - 4\lambda_1}{3p_-^2} \right), \\ \frac{4}{y} \tilde{W}_3^{(2)} + \tilde{W}_4^{(2)} + \frac{1}{y} \tilde{W}_5^{(2)} &= \frac{\delta(p_+)}{p_-} \left(\frac{2\lambda_1 + 12\lambda_2}{3p_-} - \frac{4\lambda_1 + 9\lambda_2}{m_b} \right) + \frac{\delta'(p_+)}{p_-} \left(\frac{2\lambda_1}{3} + 4\lambda_2 \right).\end{aligned}\quad (34)$$

The desired $1/(M_B - P_+)^2$ corrections to the structure functions \mathcal{F}_i can then be extracted by expanding the leading and subleading contributions $\mathcal{F}_i^{(0)}$ and $\mathcal{F}_i^{\text{hadr}(1)}$ in terms of their moments [11], and by subtracting the result from equation (34). Following the same procedure as outlined in Section 2.4 we express the result in terms of the leading shape function. This gives

$$\begin{aligned}\mathcal{F}_1^{\text{hadr}(2)}(P_+, y) &= \frac{1}{(M_B - P_+)^2} \left(\frac{4\lambda_1 - 6\lambda_2}{3y^2} + \frac{\lambda_1 + 3\lambda_2}{6} \right) \hat{S}(P_+, \mu_i), \\ \mathcal{F}_2^{\text{hadr}(2)}(P_+, y) &= \frac{1}{(M_B - P_+)^2} \left(\frac{-2\lambda_1 + 3\lambda_2}{3y^2} \right) \hat{S}(P_+, \mu_i), \\ \mathcal{F}_3^{\text{hadr}(2)}(P_+, y) &= \frac{1}{(M_B - P_+)^2} \left(\frac{4\lambda_1 + 24\lambda_2}{3y^2} - \frac{7\lambda_1 + 18\lambda_2}{3y} \right) \hat{S}(P_+, \mu_i).\end{aligned}\quad (35)$$

When using the shape function \mathcal{S} of Section 2.3 the y -independent terms in $\mathcal{F}_1^{\text{hadr}(2)}$ change. In that case, we find

$$\mathcal{F}_1^{\text{hadr}(2)}(P_+, y) = \frac{1}{(M_B - P_+)^2} \left(\frac{4\lambda_1 - 6\lambda_2}{3y^2} - \frac{5\lambda_1 + 15\lambda_2}{6} \right) \mathcal{S}(P_+, \mu_i), \quad (36)$$

while the functions $\mathcal{F}_2^{\text{hadr}(2)}$ and $\mathcal{F}_3^{\text{hadr}(2)}$ remain unchanged.

3.5 Weak annihilation corrections

In the OPE calculation several contributions appear at third order in the power expansion: $1/m_b$ corrections to the kinetic and chromo-magnetic operators, the Darwin and spin-orbit terms, and weak annihilation contributions. The Darwin and spin-orbit terms correspond to the forward B -meson matrix elements of (light) flavor-singlet operators [32]. The corresponding HQET parameters ρ_D^3 and ρ_{LS}^3 can in principle be extracted from inclusive $\bar{B} \rightarrow X_c l^- \bar{\nu}$ decays. They are insensitive to the flavor of the spectator quark inside the B meson. The weak annihilation contribution, on the other hand, results from four-quark operators with flavor non-singlet structure. They can thus be different for charged or neutral B mesons. Graphically, this contribution corresponds to a process in which the b and \bar{u} quark annihilate into a W^- . Because of the flavor dependence, this contribution would effect neutral and charged B mesons differently [33]. One choice of basis for the corresponding four-quark operators is [34]

$$\langle \bar{B} | \bar{b}_L \gamma_\mu u_L \bar{u}_L \gamma^\mu b_L | \bar{B} \rangle = \frac{f_B^2 M_B}{8} B_1, \quad \langle \bar{B} | \bar{b}_R u_L \bar{u}_L b_R | \bar{B} \rangle = \frac{f_B^2 M_B}{8} B_2, \quad (37)$$

where f_B is the B -meson decay constant and B_i are hadronic parameters. In the vacuum saturation approximation they are given by $B_1 = B_2 = 1$ for charged B mesons and $B_1 = B_2 = 0$ for neutral B mesons. The total semileptonic rate is then proportional to the difference $B_2 - B_1$, which implies that the weak annihilation contribution would vanish in this approximation.

Currently there are only estimates of the magnitude of the deviation of this difference from zero, but its effect of the total branching ratio is [35]

$$\delta B(B \rightarrow X_u l^- \bar{\nu}) \approx 3.9 \left(\frac{f_B}{0.2 \text{ GeV}} \right)^2 \left(\frac{B_2 - B_1}{0.1} \right) |V_{ub}|^2. \quad (38)$$

Again, we expect this effect to be different for charged and neutral B mesons. The most important feature of weak annihilation is that it is formally concentrated at the kinematical point where all the momentum of the heavy quark is transferred to the lepton pair [33]. At the parton level this implies that the corresponding contribution is proportional to $\delta(q^2 - m_b^2)$. It is therefore included in every cut that includes the q^2 endpoint, and its effect is independent of the specific form of the cut.

We suggest two different strategies to control this effect. The first is to include it as a constant contribution proportional to the total rate. A recent study [36] puts a limit on this effect of $\pm 1.8\%$ on the total rate at one standard deviation by analyzing CLEO data. The second one is to impose a cut $q^2 \leq q_{\text{max}}^2$, thus avoiding the region where the weak annihilation contribution is concentrated. The maximal value of q^2 is $(M_B - M_\pi)^2$, but one must exclude a larger region of phase space, such that the *excluded* portion at large q^2 (corresponding to a region near the origin in the (P_-, P_+) plane) can be reliably calculated using OPE methods. In our numerical analysis, we will study the effect of a cut $q^2 \leq (M_B - M_D)^2$, which satisfies this criterion.

4 Shape-function parameterizations

Hadronic-physics effects enter the description of inclusive decay rates via non-perturbative shape functions. Perturbation theory cannot tell us much about the local form of these functions, but moments of them are calculable provided that the domain of integration is much larger than Λ_{QCD} . Since the shape functions contain much information about the internal structures of the b quark inside the B meson, knowledge of them relates directly to the determination of the b -quark mass m_b , the kinetic energy λ_1 , and, in principle, the matrix elements of higher-dimensional operators. Improved measurements of the shape of the $\bar{B} \rightarrow X_s \gamma$ photon spectrum will therefore lead directly to a more precise determination of HQET parameters. On the other hand, this argument is commonly turned around to constrain the leading shape function using knowledge of m_b and λ_1 from other physical processes such as a $b \rightarrow c$ moment analysis [37]. We emphasize, however, that there obviously exist infinitely many locally different functions that have identical first few moments. In this section we present a few functional forms that can be used to model the shape functions and to fit the current experimental data.

To achieve stringent constraints a precise definition of the HQET parameters is required. It is a well-known fact that the pole-mass scheme introduces uncontrollable ambiguities. To avoid these uncertainties several short-distance definitions have been proposed, such as the $\overline{\text{MS}}$ scheme, the potential-subtraction scheme [38], the $\Upsilon(1S)$ scheme [39], the kinetic scheme [40], or the shape-function scheme [7]. While the decay rates are of course independent of the particular choice, it is advantageous to use a mass scheme that is designed for the physics

problem at hand. In the case of inclusive B decays into light particles, this is the shape-function scheme.

4.1 Models for the leading shape function

4.1.1 Moment relations in the shape-function scheme

Moments of $\hat{S}(\hat{\omega}, \mu_i)$ are defined with an upper limit of integration $\hat{\omega}_0$. For practical applications, $\hat{\omega}_0$ should be thought of as the size of the window where the $\bar{B} \rightarrow X_s \gamma$ photon spectrum is experimentally accessible, e.g. $\hat{\omega}_0 = M_B - 2E_\gamma^{min}$ with $E_\gamma^{min} \approx 1.8$ GeV. Following [7], we define

$$M_N(\hat{\omega}_0, \mu_i) \equiv \int_0^{\hat{\omega}_0} d\hat{\omega} \hat{\omega}^N \hat{S}(\hat{\omega}, \mu_i). \quad (39)$$

These moments can be expanded in terms of matrix elements of local operators as long as $\hat{\omega}_0$ is much larger than Λ_{QCD} . The shape-function scheme defines these HQET parameters implicitly through the moment relations to all orders in perturbation theory,

$$\begin{aligned} \frac{M_1(\mu_f + \bar{\Lambda}(\mu_f, \mu_i), \mu_i)}{M_0(\mu_f + \bar{\Lambda}(\mu_f, \mu_i), \mu_i)} &= \bar{\Lambda}(\mu_f, \mu_i), \\ \frac{M_2(\mu_f + \bar{\Lambda}(\mu_f, \mu_i), \mu_i)}{M_0(\mu_f + \bar{\Lambda}(\mu_f, \mu_i), \mu_i)} &= \frac{\mu_\pi^2(\mu_f, \mu_i)}{3} + \bar{\Lambda}^2(\mu_f, \mu_i), \end{aligned} \quad (40)$$

etc. Here, the factorization scale μ_f is much larger than Λ_{QCD} , and reflects the fact that the value of the parameters depend on the size of integration domain $\hat{\omega}_0 = \mu_f + \bar{\Lambda}(\mu_f, \mu_i)$. In practice μ_f is close to the intermediate scale μ_i . At tree level, the relations between parameters in the shape-function scheme and the pole scheme are $\bar{\Lambda}(\mu_f, \mu_i) = \bar{\Lambda}^{\text{pole}}$, $\mu_\pi^2(\mu_f, \mu_i) = -\lambda_1$, etc. They have been worked out to two-loop order in [41], which allows for a precise determination of $\bar{\Lambda}(\mu_f, \mu_i)$ and $\mu_\pi^2(\mu_f, \mu_i)$ from other physical processes.

For reference purposes, it is helpful to quote values for the b -quark mass and μ_π^2 using only a single scale μ_* instead of two independent scales μ_f and μ_i . To one-loop order, these parameters can be related to those determined from the moments via [7]

$$\begin{aligned} m_b^{\text{SF}}(\mu_*, \mu_*) &= M_B - \bar{\Lambda}(\mu_f, \mu_i) - \mu_* \frac{C_F \alpha_s(\mu_*)}{\pi} + \mu_f \frac{C_F \alpha_s(\mu_i)}{\pi} \left[1 - 2 \ln \frac{\mu_f}{\mu_i} + \frac{2}{3} \frac{\mu_\pi^2(\mu_f, \mu_i)}{\mu_f^2} \right], \\ \mu_\pi^2(\mu_*, \mu_*) &= \mu_\pi^2(\mu_f, \mu_i) \left[1 + \frac{C_F \alpha_s(\mu_*)}{2\pi} - \frac{C_F \alpha_s(\mu_i)}{\pi} \left\{ \frac{1}{2} + 3 \left(1 - \frac{\mu_f^2}{\mu_\pi^2(\mu_f, \mu_i)} \right) \ln \frac{\mu_f}{\mu_i} \right\} \right], \end{aligned} \quad (41)$$

where we have neglected higher-dimensional operator matrix elements that are suppressed by inverse powers of μ_f . A typical choice for the scale μ_* is 1.5 GeV.

The general procedure for modeling the leading shape function $\hat{S}(\hat{\omega}, \mu_i)$ from a given functional form $F(\hat{\omega})$ is as follows. The shape of $F(\hat{\omega})$ is assumed to be tunable so that it can be used to fit the $\bar{B} \rightarrow X_s \gamma$ photon spectrum. Only the norm of the shape function remains to be fixed. Note that the moment relations (40) are insensitive to the norm, so that formulae

for $\bar{\Lambda}$ and μ_π^2 follow directly from the functional form of $F(\hat{\omega})$. Examples of such formulae will be given below. We define moments $M_N^{[F]}(\hat{\omega}_0)$ of F in analogy with (39). The first relation in (40) implies that for a given $\hat{\omega}_0$ the factorization scale is

$$\mu_f = \hat{\omega}_0 - \frac{M_1^{[F]}(\hat{\omega}_0)}{M_0^{[F]}(\hat{\omega}_0)}. \quad (42)$$

Now that μ_f is known, the norm is determined by requiring that the zeroth moment of the shape function is [7]

$$M_0(\hat{\omega}_0, \mu_i) = 1 - \frac{C_{F\alpha_s}(\mu_i)}{\pi} \left(\ln^2 \frac{\mu_f}{\mu_i} + \ln \frac{\mu_f}{\mu_i} + \frac{\pi^2}{24} \right) + \frac{C_{F\alpha_s}(\mu_i)}{\pi} \left(\ln \frac{\mu_f}{\mu_i} - \frac{1}{2} \right) \frac{\mu_\pi^2(\mu_f, \mu_i)}{3\mu_f^2} + \dots \quad (43)$$

It follows that $[M_0(\hat{\omega}_0, \mu_i)/M_0^{[F]}(\hat{\omega}_0)] F(\hat{\omega})$ serves as a model of $\hat{S}(\hat{\omega}, \mu_i)$.

4.1.2 Three models

We will now suggest three two-parameter models for the leading order shape function based on an exponential-type function $F^{(\text{exp})}$, a gaussian-type function $F^{(\text{gauss})}$, and hyperbolic-type function $F^{(\text{hyp})}$. We use two parameters that can be tuned to fit the photon spectrum: a dimensionful quantity Λ which characterizes the position of the average $\langle \hat{\omega} \rangle$, and a positive number b which governs the behavior for small $\hat{\omega}$. They are

$$\begin{aligned} F^{(\text{exp})}(\hat{\omega}; \Lambda, b) &= \frac{N^{(\text{exp})}}{\Lambda} \left(\frac{\hat{\omega}}{\Lambda} \right)^{b-1} \exp \left(-d_{(\text{exp})} \frac{\hat{\omega}}{\Lambda} \right), \\ F^{(\text{gauss})}(\hat{\omega}; \Lambda, b) &= \frac{N^{(\text{gauss})}}{\Lambda} \left(\frac{\hat{\omega}}{\Lambda} \right)^{b-1} \exp \left(-d_{(\text{gauss})} \frac{\hat{\omega}^2}{\Lambda^2} \right), \\ F^{(\text{hyp})}(\hat{\omega}; \Lambda, b) &= \frac{N^{(\text{hyp})}}{\Lambda} \left(\frac{\hat{\omega}}{\Lambda} \right)^{b-1} \cosh^{-1} \left(d_{(\text{hyp})} \frac{\hat{\omega}}{\Lambda} \right). \end{aligned} \quad (44)$$

For convenience, we normalize these functions to unity. The parameters $d_{(i)}$ are determined by the choice $\Lambda = \langle \hat{\omega} \rangle$. For given parameters Λ and b we find

$$\begin{aligned} N^{(\text{exp})} &= \frac{d_{(\text{exp})}^b}{\Gamma(b)}, & d_{(\text{exp})} &= b, \\ N^{(\text{gauss})} &= \frac{2 d_{(\text{gauss})}^{b/2}}{\Gamma(b/2)}, & d_{(\text{gauss})} &= \left(\frac{\Gamma(\frac{1+b}{2})}{\Gamma(\frac{b}{2})} \right)^2, \\ N^{(\text{hyp})} &= \frac{[4 d_{(\text{hyp})}]^b}{2 \Gamma(b) [\zeta(b, \frac{1}{4}) - \zeta(b, \frac{3}{4})]}, & d_{(\text{hyp})} &= \frac{b}{4} \frac{\zeta(1+b, \frac{1}{4}) - \zeta(1+b, \frac{3}{4})}{\zeta(b, \frac{1}{4}) - \zeta(b, \frac{3}{4})}, \end{aligned} \quad (45)$$

where $\zeta(b, a) = \sum_{k=0}^{\infty} (k+a)^{-b}$ is the generalized Riemann zeta function.

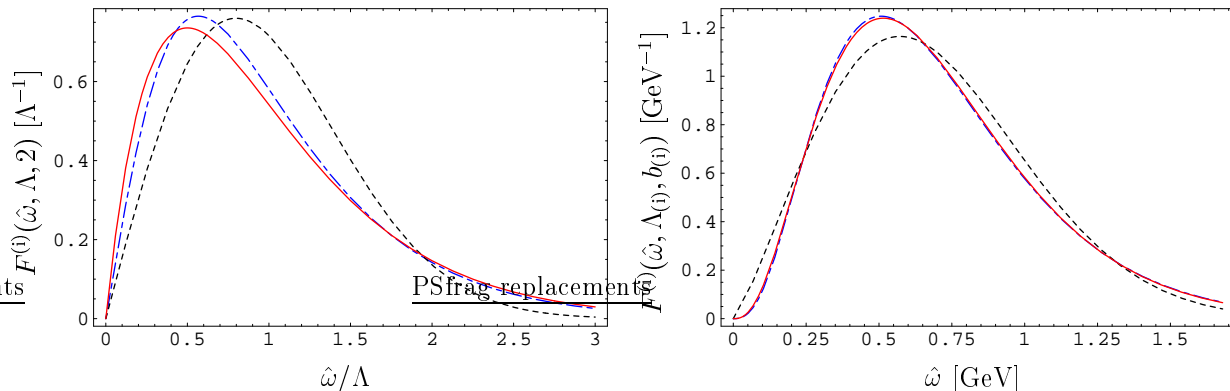


Figure 2: **LEFT:** Three different models with linear onset for small $\hat{\omega}$. We show $F^{(\text{exp})}(\hat{\omega}, \Lambda, 2)$ (solid), $F^{(\text{gauss})}(\hat{\omega}, \Lambda, 2)$ (dotted), and $F^{(\text{hyp})}(\hat{\omega}, \Lambda, 2)$ (dash-dotted). **RIGHT:** The same functions with the parameters Λ and b tuned such that $m_b^{\text{SF}}(\mu_*, \mu_*) = 4.63$ GeV and $\mu_\pi^2(\mu_*, \mu_*) = 0.2$ GeV² at the reference scale $\mu_* = 1.5$ GeV. See text for explanation.

An illustration of the functional forms of the models is given on the left-hand side in Figure 2. We show a plot with the choice $b = 2$, i.e. a linear onset for small $\hat{\omega}$. For realistic scenarios b is typically somewhat larger than 2, which means that the onset is slower than linear. Since the hyperbolic model approaches the exponential curve for large values of b , we nevertheless show the curves with $b = 2$, so that differences are visible.

For the first two models, analytic expressions for the HQET parameters $\bar{\Lambda}$ and μ_π^2 are available. Following the discussion above, we compute the moments over the interval $[0, \hat{\omega}_0]$ and find for the exponential form $F^{(\text{exp})}(\hat{\omega}; \Lambda, b)$

$$\begin{aligned} \bar{\Lambda}(\mu_f, \mu_i) &= \frac{\Lambda}{b} \frac{\Gamma(1+b) - \Gamma(1+b, \frac{b\hat{\omega}_0}{\Lambda})}{\Gamma(b) - \Gamma(b, \frac{b\hat{\omega}_0}{\Lambda})}, \\ \mu_\pi^2(\mu_f, \mu_i) &= 3 \left[\frac{\Lambda^2}{b^2} \frac{\Gamma(2+b) - \Gamma(2+b, \frac{b\hat{\omega}_0}{\Lambda})}{\Gamma(b) - \Gamma(b, \frac{b\hat{\omega}_0}{\Lambda})} - \bar{\Lambda}(\mu_f, \mu_i)^2 \right], \end{aligned} \quad (46)$$

where $\mu_f = \hat{\omega}_0 - \bar{\Lambda}(\mu_f, \mu_i)$. A similar calculation for the gaussian form $F^{(\text{gauss})}(\hat{\omega}; \Lambda, b)$ yields

$$\begin{aligned} \bar{\Lambda}(\mu_f, \mu_i) &= \frac{\Lambda}{\sqrt{d_{(\text{gauss})}}} \frac{\Gamma(\frac{1+b}{2}) - \Gamma(\frac{1+b}{2}, \frac{d_{(\text{gauss})}\hat{\omega}_0^2}{\Lambda^2})}{\Gamma(\frac{b}{2}) - \Gamma(\frac{b}{2}, \frac{d_{(\text{gauss})}\hat{\omega}_0^2}{\Lambda^2})}, \\ \mu_\pi^2(\mu_f, \mu_i) &= 3 \left[\frac{\Lambda^2}{d_{(\text{gauss})}} \frac{\Gamma(1+\frac{b}{2}) - \Gamma(1+\frac{b}{2}, \frac{d_{(\text{gauss})}\hat{\omega}_0^2}{\Lambda^2})}{\Gamma(\frac{b}{2}) - \Gamma(\frac{b}{2}, \frac{d_{(\text{gauss})}\hat{\omega}_0^2}{\Lambda^2})} - \bar{\Lambda}(\mu_f, \mu_i)^2 \right]. \end{aligned} \quad (47)$$

For the hyperbolic form $F^{(\text{hyp})}(\hat{\omega}; \Lambda, b)$ the procedure can be performed numerically.

Ultimately the shape function should be fitted to the $\bar{B} \rightarrow X_s \gamma$ photon spectrum, and the above equations then determine $\bar{\Lambda}$ and μ_π^2 . On the other hand, these formulae can be inverted

to determine Λ and b from the current values of HQET parameters. For example, if we were to adopt the values $m_b^{\text{SF}}(\mu_*, \mu_*) = 4.63 \text{ GeV}$ and $\mu_\pi^2(\mu_*, \mu_*) = 0.20 \text{ GeV}^2$ for diagonal scale setting (41) at $\mu_* = 1.5 \text{ GeV}$, we would find the parameter pair $\Lambda \approx 0.70 \text{ GeV}$, $b \approx 3.72$ for the exponential model, $\Lambda \approx 0.69 \text{ GeV}$, $b \approx 2.23$ for the gaussian model, and $\Lambda \approx 0.71 \text{ GeV}$, $b \approx 3.57$ for the hyperbolic model. On the right-hand side of Figure 2 we show these three different curves, plotted over the interval $[0, \hat{\omega}_0]$, over which the moment constraints are imposed. While the exponential curve (solid) and the hyperbolic function (dash-dotted) are barely distinguishable, the gaussian model has quite different characteristics. It is broader, almost linear at the onset, faster to fall off, and the maximum is shifted toward larger $\hat{\omega}$.

In most applications, shape functions are needed for arguments $\hat{\omega}$ of order Λ_{QCD} . However, in some cases, like the ideal cut on hadronic invariant mass, $\hat{\omega}$ is required to be as large as M_D , which is much larger than Λ_{QCD} . This “tail” of the shape function can be computed using perturbation theory and is for the leading shape function [7]

$$\hat{S}(\hat{\omega} \gg \Lambda_{\text{QCD}}, \mu) = -\frac{C_F \alpha_s(\mu)}{\pi} \frac{1}{\hat{\omega} - \bar{\Lambda}} \left[\left(2 \ln \frac{\hat{\omega} - \bar{\Lambda}}{\mu} + 1 \right) + \frac{2\mu_\pi^2}{3(\hat{\omega} - \bar{\Lambda})^2} \left(\ln \frac{\hat{\omega} - \bar{\Lambda}}{\mu} - 1 \right) + \dots \right]. \quad (48)$$

The shape function is needed at the renormalization scale $\mu = \mu_i$, which implies that the coupling $\alpha_s(\mu)$ is perturbative. Note that this radiative tail tends asymptotically to zero slower than $\hat{\omega}^{-1}$ and is negative. It follows that the shape function must go through zero somewhere near $\hat{\omega} \sim \text{few } \Lambda_{\text{QCD}}$. For practical purposes, the above expressions can be “glued” onto models of the non-perturbative regime using some transition function that switches from zero to one in the vicinity of $\hat{\omega} \sim \bar{\Lambda} + \mu_i/\sqrt{e}$, where the leading term in (48) vanishes. However, we stress that for applications with a maximal P_+ not larger than about 1.6 GeV the radiative tail of the shape function is not required.

4.2 Models for subleading shape functions

In the last section we have been guided by the fact that the $\bar{B} \rightarrow X_s \gamma$ photon spectrum is at leading power directly determined by the leading shape function. This helped in finding models that have roughly the same shape as the photon spectrum. At the subleading level considered here, however, no such guidance is provided to us. The available information is limited to the tree-level moment relations, namely that their norms vanish while their first moments do not. It is conventional to defined “unhatted versions” of each shape function, e.g. $t(\omega)$, where it is understood that $\hat{t}(\hat{\omega}) = t(\bar{\Lambda}_\infty - \hat{\omega})$, where $t(\omega)$ has support on the interval $-\infty < \omega < \bar{\Lambda}_\infty$, and $\bar{\Lambda}_\infty$ is the asymptotic value of the difference ($M_B - m_b$) in the heavy-quark limit (see [11] for a detailed discussion). The moment relations then take the form [20]

$$t(\omega) = \lambda_2 \delta'(\omega) + \dots, \quad u(\omega) = -\frac{2\lambda_1}{3} \delta'(\omega) + \dots, \quad v(\omega) = -\lambda_2 \delta'(\omega) + \dots \quad (49)$$

In [11], two classes of models have been proposed. In both approaches the subleading shape functions are “derived” from the leading (unhatted) shape function $S(\omega)$. The first one treats the subleading shape functions as proportional to $\omega S(\omega)$, and the second class leaves them proportional to the derivative $S'(\omega)$. The proportionality constants are chosen so as to fulfill

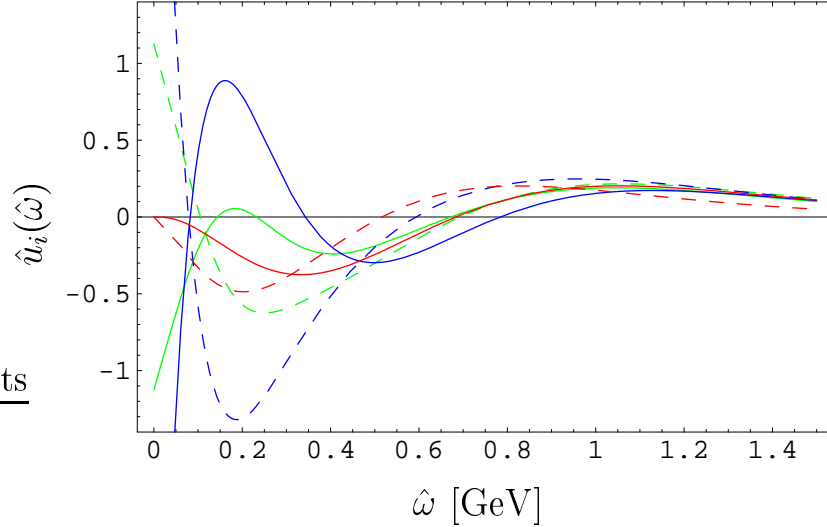


Figure 3: Models for the subleading shape function $\hat{u}(\hat{\omega})$. The parameters were chosen such that the resulting functions have the characteristics of subleading shape functions, meaning that $\hat{u}(\hat{\omega}) = O(1)$ for $\hat{\omega} = O(\Lambda_{\text{QCD}})$, whereas the functions must fall off quickly once $\hat{\omega}$ exceeds values of about 1 GeV. Specifically, we used $M_2 = (0.3 \text{ GeV})^3$, $a^{(N)} = 5$, and $a^{(\text{BIK})} = 10$.

the above moment relation. This procedure yields the following models:

$$\hat{t}_1(\hat{\omega}) = \frac{3\lambda_2}{\lambda_1} (\bar{\Lambda} - \hat{\omega}) \hat{S}(\hat{\omega}), \quad \hat{u}_1(\hat{\omega}) = -2(\bar{\Lambda} - \hat{\omega}) \hat{S}(\hat{\omega}), \quad \hat{v}_1(\hat{\omega}) = -\frac{3\lambda_2}{\lambda_1} (\bar{\Lambda} - \hat{\omega}) \hat{S}(\hat{\omega}), \quad (50)$$

and

$$\hat{t}_2(\hat{\omega}) = -\lambda_2 \hat{S}'(\hat{\omega}), \quad \hat{u}_2(\hat{\omega}) = \frac{2\lambda_1}{3} \hat{S}'(\hat{\omega}), \quad \hat{v}_2(\hat{\omega}) = \lambda_2 \hat{S}'(\hat{\omega}). \quad (51)$$

Below, we will sometimes refer to the first set of functions as the “default choice”. Since at tree level all mass schemes are equivalent to each other, there is no unique prescription in choosing the values of λ_i . For consistency we will use $\bar{\Lambda} = \bar{\Lambda}(\mu_f, \mu_i)$, $\lambda_1 = -\mu_\pi^2(\mu_*, \mu_*)$, and $\lambda_2 = 0.12 \text{ GeV}^2$.

There are of course infinitely many possibilities to find models for subleading shape functions that are in accordance with (49). For example, the difference of any two models for the leading shape function has by definition zero norm and first two moments. Such a function can be arbitrarily added to any model without violating the moment relations. Here, in the case of subleading shape functions, we only need to take functions into account that have vanishing norm and first moment.

Several such functions have been proposed in recent work on subleading shape functions,

see e.g. [11, 23, 25, 42]. Specifically, let us define

$$\begin{aligned}
h^{(\text{N})}(\hat{\omega}) &\equiv \frac{M_2}{\Omega_0^3} \left\{ \frac{a^3}{2} e^{-az} \left(1 - 2az + \frac{a^2 z^2}{2} \right) \right\}, \\
h^{(\text{GN})}(\hat{\omega}) &\equiv \frac{M_2}{\Omega_0^3} \left\{ \left[\frac{2\sqrt{\pi a}}{\pi - 2} e^{-az^2} \left(1 - 2z\sqrt{\frac{a}{\pi}} \right) \right] - 2e^{-z} + 2z e^{-2z} \text{Ei}(z) \right\}, \\
h^{(\text{BIK})}(\hat{\omega}) &\equiv \frac{M_2}{\Omega_0^3} \left\{ \left[\frac{\pi^2}{4} \frac{2\sqrt{\pi a}}{\pi - 2} e^{-az^2} \left(1 - 2z\sqrt{\frac{a}{\pi}} \right) \right] \right. \\
&\quad \left. + \frac{8}{(1+z^2)^4} \left[z \ln z + \frac{z}{2} (1+z^2) - \frac{\pi}{4} (1-z^2) \right] \right\}, \tag{52}
\end{aligned}$$

where $z = \hat{\omega}/\Omega_0$, and the reference quantity Ω_0 depends on the type of function, namely $\Omega_0^{(\text{N})} = \bar{\Lambda}$, $\Omega_0^{(\text{GN})} = \frac{2}{3}\bar{\Lambda}$, and $\Omega_0^{(\text{BIK})} = \frac{8}{3\pi}\bar{\Lambda}$. The quantity a is a free parameter. The functions (52) have by construction vanishing norm and first moment. The second moments are proportional to the prefactor M_2 , which can be fixed such that all three functions have the same second moment, which is parametrically of order $(\Lambda_{\text{QCD}})^3$. The values for the parameters a and M_2 should be chosen such that the following characteristics of subleading shape functions are respected: First, they are dimensionless functions, so that their values are naturally of $O(1)$ for $\hat{\omega} \sim \Lambda_{\text{QCD}}$. Secondly, when integrated over a sufficiently large domain, their contributions are determined in terms of their first few moments. In particular, this implies that for values of $\hat{\omega} \gg \Lambda_{\text{QCD}}$ the integrals over the subleading shape functions must approach zero.

Given the three functions (52), we construct several new sets of models of the form $\{\hat{t} \pm h^{(i)}, \hat{u} \mp h^{(i)}, \hat{v} \pm h^{(i)}\}$. As an example, we use the following four new sets of subleading shape function models:

$$\begin{aligned}
\hat{t}_3(\hat{\omega}) &= \hat{t}_1(\hat{\omega}) - h^{(\text{N})}(\hat{\omega}), & \hat{u}_3(\hat{\omega}) &= \hat{u}_1(\hat{\omega}) + h^{(\text{N})}(\hat{\omega}), & \hat{v}_3(\hat{\omega}) &= \hat{v}_1(\hat{\omega}) - h^{(\text{N})}(\hat{\omega}), \\
\hat{t}_4(\hat{\omega}) &= \hat{t}_2(\hat{\omega}) + h^{(\text{N})}(\hat{\omega}), & \hat{u}_4(\hat{\omega}) &= \hat{u}_2(\hat{\omega}) - h^{(\text{N})}(\hat{\omega}), & \hat{v}_4(\hat{\omega}) &= \hat{v}_2(\hat{\omega}) + h^{(\text{N})}(\hat{\omega}), \\
\hat{t}_5(\hat{\omega}) &= \hat{t}_1(\hat{\omega}) - h^{(\text{BIK})}(\hat{\omega}), & \hat{u}_5(\hat{\omega}) &= \hat{u}_1(\hat{\omega}) + h^{(\text{BIK})}(\hat{\omega}), & \hat{v}_5(\hat{\omega}) &= \hat{v}_1(\hat{\omega}) - h^{(\text{BIK})}(\hat{\omega}), \\
\hat{t}_6(\hat{\omega}) &= \hat{t}_2(\hat{\omega}) + h^{(\text{BIK})}(\hat{\omega}), & \hat{u}_6(\hat{\omega}) &= \hat{u}_2(\hat{\omega}) - h^{(\text{BIK})}(\hat{\omega}), & \hat{v}_6(\hat{\omega}) &= \hat{v}_2(\hat{\omega}) + h^{(\text{BIK})}(\hat{\omega}).
\end{aligned} \tag{53}$$

Note that for these new functions we no longer have $\hat{t}(\hat{\omega}) = -\hat{v}(\hat{\omega})$, which is an ‘‘accidental’’ feature of the first two models (50) and (51). The fact that the two functions have equal (but opposite in sign) first moments does not imply that this should be the case.

We display the six different models for $\hat{u}(\hat{\omega})$ in Figure 3, where we have used the exponential-type model (44) for $\hat{S}(\hat{\omega})$. In the region $\hat{\omega} \sim \Lambda_{\text{QCD}}$ they differ dramatically from each other, while the large $\hat{\omega}$ dependence is dominated by the moment relations (49). In practice we can use this set of models to estimate the dependence of rates on subleading shape functions.

4.3 Illustrative studies and embellishments

We stressed several times that the calculation of the hadronic tensor is optimized for the shape-function region of large P_- and small P_+ . This is to be understood as the sizes of

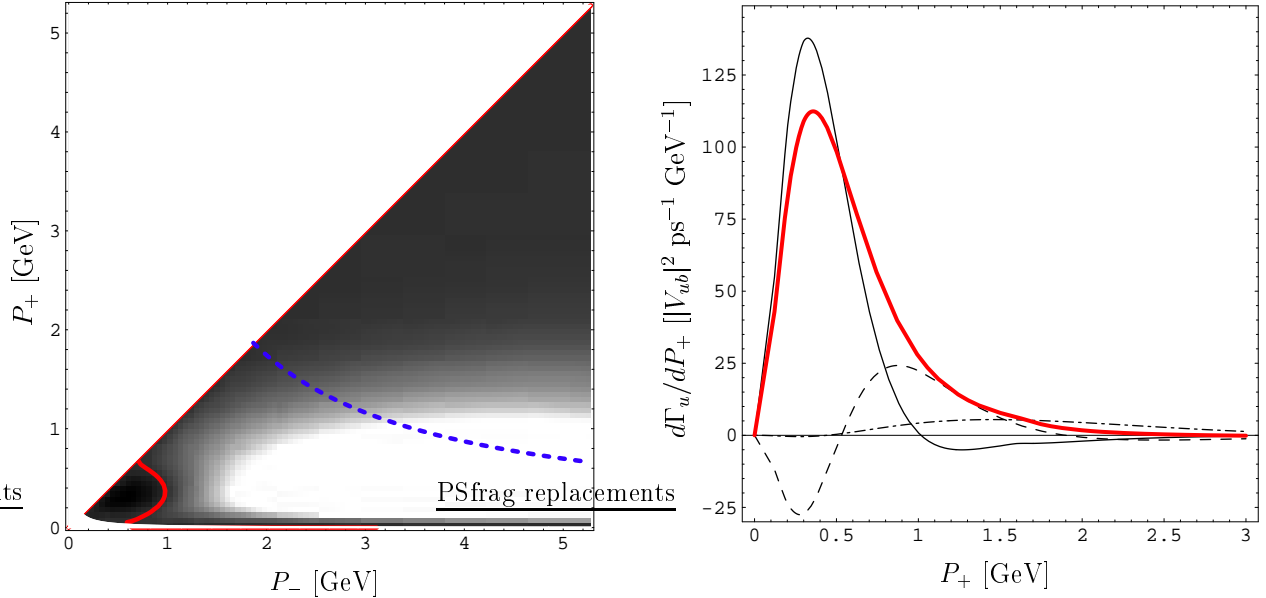


Figure 4: LEFT: A graphical representation of the hadronic phase space and the theoretical predictions for the triple differential decay rate, which is “optimized” for the shape-function region and extended over the entire phase space. The light area represents a large and positive decay rate. Black regions denote areas where the decay rate is close to zero. The dotted line is given by $P_+ P_- = M_D^2$, which means that charmed background is located in the upper wedge. See text for further explanation. RIGHT: The P_+ spectrum extended to large values of P_+ . The thin solid line denotes the leading power prediction, the dashed line depicts first-order power corrections, and the dash-dotted line second-order power corrections. The thick solid line is their sum.

integration domains for P_- and P_+ , since it is hopeless to calculate the differential decay rate point-by-point without heavily violating quark-hadron duality. Nevertheless, it is interesting to study how the result extends over the entire phase space. To this end we integrate the triple differential decay rate (21) over the leptonic variable $P_+ \leq P_l \leq P_-$, which yields the exact formula

$$\frac{d^2\Gamma_u}{dP_+ dP_-} = \frac{G_F^2 |V_{ub}|^2}{96\pi^3} U_y(\mu_h, \mu_i) (M_B - P_+) (P_- - P_+)^2 \times \left\{ (3M_B - 2P_- - P_+) \mathcal{F}_1 + 6(M_B - P_-) \mathcal{F}_2 + (P_- - P_+) \mathcal{F}_3 \right\}. \quad (54)$$

Using the default settings and shape functions presented in Section 4 we can depict the theoretical predictions for the double differential decay rate (54), which is shown on the left-hand side of Figure 4. Note that we needed to include the radiative tail of the shape function to the model, so as to include larger values of P_+ . For very small P_- values the rate turns negative (to the left of the red line in the figure), signaling a breakdown of quark-hadron duality. It is reassuring that the only region where this happens is the “resonance region” of very small P_- , where the hadronic invariant mass is of order Λ_{QCD} . Theoretical calculations

of inclusive decay distributions can only be trusted when a sufficiently large region of phase space containing many hadronic final states is included.

Another useful quantity to consider is the differential P_+ rate, which is obtained by integrating the double differential rate over $P_+ \leq P_- \leq M_B$. We plot the resulting P_+ spectrum over a large domain, which is shown on the right-hand side of Figure 4. In the plot we also disentangle the contributions from different levels in power counting, which shows how the convergence of the power series works.

5 Predictions and error estimates for partial rates

Before discussing predictions for partial $\bar{B} \rightarrow X_u l^- \bar{\nu}$ rates for various experimental cuts, let us recapitulate the ingredients of the calculation and general procedure. We have presented expressions for the triple differential decay rate, which have been organized in inverse powers of $(M_B - P_+)$. The leading-power contribution is given to one-loop order in renormalization-group improved perturbation theory. At first subleading power two contributions arise. The first type involves subleading shape functions and is included at tree level, while the second type contributes perturbative corrections of order α_s that come with the leading shape function. Further contributions enter at second subleading power and are again of the two types: perturbative corrections of order α_s and non-perturbative structures at tree level. In summary, partial rates are computed term-by-term and the result can be written as

$$\Gamma_u = \Gamma_u^{(0)} + (\Gamma_u^{\text{kin}(1)} + \Gamma_u^{\text{hadr}(1)}) + (\Gamma_u^{\text{kin}(2)} + \Gamma_u^{\text{hadr}(2)}) + \dots \quad (55)$$

The goal of this section is to both test the convergence of this series and to perform a thorough analysis of uncertainties. We mentioned many times before that the procedure should be to fit the leading shape function to the $\bar{B} \rightarrow X_s \gamma$ photon spectrum. Therefore the central value and leading shape function uncertainty are determined by experiment. In this section we will adopt a model for the leading shape function, which is the exponential-type model in (44) with $m_b^{\text{SF}}(\mu_*, \mu_*) = 4.63 \text{ GeV}$ and $\mu_\pi^2(\mu_*, \mu_*) = 0.2 \text{ GeV}^2$ at $\mu_* = 1.5 \text{ GeV}$, and study all remaining errors. The aforementioned example is close to the two-loop values given in [41]. However, to illustrate the dependence on this particular choice we also provide tables based on a shape-function parameters $m_b^{\text{SF}}(\mu_*, \mu_*) = 4.57 \text{ GeV}$ and $\mu_\pi^2(\mu_*, \mu_*) = 0.3 \text{ GeV}^2$, which are closer to the one-loop values obtained in that paper. While we expect the central value and the leading shape-function uncertainty to change as the experimental data becomes more precise, the remaining errors would differ only marginally. They are coming from several sources.

First, there are uncertainties associated with the functional forms of subleading shape functions. To estimate them, we take the spread of results when using the six different models of Section 4.2. The central value for a partial decay rate is quoted using the center of the spread from subleading shape functions, i.e., not necessarily given by the default models \hat{t}_1 , \hat{u}_1 , \hat{v}_1 . Secondly, there are perturbative uncertainties associated with the setting of the matching scales μ_h , μ_i , or $\bar{\mu}$. Decay rates are formally independent of them. However, a dependence is picked up by truncating the perturbative series, so that a variation of the scales serves as an estimate of higher-order perturbative corrections. Some comments are in order.

- The hard scale μ_h is of order m_b . In perturbative logarithms the scale appears in the combination (ym_b/μ_h) , see (24) and (27). To set a central value for μ_h we are guided by the average $\langle y \rangle m_b$. The leading term for the double differential decay rate $d^2\Gamma_u/dP_+dy$ is proportional to $y^2(3-2y)$. It follows that the average y on the interval $[0,1]$ is 0.7. However, in some applications y is not integrated over the full domain. In the error analysis we will proceed as follows: we set the central value of $\mu_h = m_b/\sqrt{2}$, which is very close to $0.7m_b$, and vary the scale from $m_b/2$ to m_b . For the central value $\alpha_s(\mu_h) \approx 0.248$.
- The intermediate scale μ_i is of order $\sqrt{m_b\Lambda_{\text{QCD}}}$. This is the renormalization scale for the shape functions and the jet function, and also enters the Sudakov factor. We fix this scale to the value $\mu_i = 1.5 \text{ GeV}$. In principle μ_i could be varied, in which case the solution of the renormalization-group equation for the shape function must be used [7, 17]. However, here we argue that when setting μ_i to a different value, the shape function should be fitted again to the photon spectrum, which makes the renormalization-group evolution obsolete. The only place where the intermediate scale has a direct impact on the extraction of $|V_{ub}|$ is through the norm of the shape function (43), which is multiplicative. In the analysis we therefore estimate the uncertainty by assigning the value $\pm(\frac{\alpha_s(\mu_i)}{\pi})^2$ as a relative error. We have $\alpha_s(\mu_i) \approx 0.357$.
- The scale $\bar{\mu}$ appears as the argument of α_s in the perturbative contributions Γ_u^{pert} . In these contributions large logarithms have not been properly resummed and $\bar{\mu}$ is thought of being somewhere in between the hard scale and Λ_{QCD} . We vary $\bar{\mu}$ from $\mu_i/\sqrt{2}$ to $\mu_i\sqrt{2}$ with the central value $\bar{\mu} = \mu_i = 1.5 \text{ GeV}$.

These three errors are added in quadrature and assigned to be the perturbative uncertainty. Finally, we need to estimate the effects from higher-dimensional operators at third and higher-order in power counting. The most prominent examples of such contributions are weak annihilation effects, which we discussed in Section 3.5. If the considered cut includes the region of phase space near the origin $P_+ \sim P_- \sim \Lambda_{\text{QCD}}$ one should assign an error, which is of a fixed value for partial decay rates. As an example one could assign $\pm 1.8\%$ of the total rate to it [36]. In principle one could avoid the uncertainty from weak annihilation by imposing a cut $q^2 \leq q_{\text{max}}^2$.

In the following we will focus on the remaining theoretical uncertainties. We quote values for the partial rates Γ_u in units of $|V_{ub}|^2 \text{ ps}^{-1}$. To convert the results to partial branching fractions the numbers need to be multiplied by $|V_{ub}|^2$ and the B -meson lifetime τ_B (in units of ps). For the total decay rate we find $\Gamma_u \approx 79 |V_{ub}|^2 \text{ ps}^{-1} (m_b/4.63 \text{ GeV})^5$, with $m_b \equiv m_b^{\text{SF}}(\mu_*, \mu_*)$ at the reference scale $\mu_* = 1.5 \text{ GeV}$, so that weak annihilation effects can be estimated to be approximately $\pm 1.4 |V_{ub}|^2 \text{ ps}^{-1}$. If desired, this error can be added in quadrature to the uncertainties stated below.

5.1 Lepton energy endpoint

A commonly used variable to discriminate against the charm background is the charged-lepton energy E_l . As long as one requires that E_l is bigger than $(M_B^2 - M_D^2)/2M_B$ the final hadronic

Table 1: Partial decay rate $\Gamma_u(E_0)$ for a cut on lepton energy $E_l > E_0$ in the B -meson rest frame, given in units of $|V_{ub}|^2 \text{ps}^{-1}$. Predictions are based on the shape-function parameter values $m_b(\mu_*, \mu_*) = 4.63 \text{ GeV}$ and $\mu_\pi^2(\mu_*, \mu_*) = 0.2 \text{ GeV}^2$.

E_0 [GeV]	Mean	subl. SF	pert.	Total
1.9	27.69	± 0.36	+2.16 -1.83	+2.19 -1.86
2.0	21.30	± 0.39	+1.54 -1.32	+1.59 -1.38
2.1	15.04	± 0.45	+0.96 -0.84	+1.06 -0.95
2.2	9.25	± 0.60	+0.49 -0.43	+0.78 -0.74
2.3	4.44	± 0.86	+0.20 -0.16	+0.89 -0.88
2.4	1.29	± 0.86	+0.05 -0.06	+0.86 -0.87

Table 2: Partial decay rate $\gamma \Gamma_u(E_0)$ for a cut on lepton energy $E_l > E_0$ in the $\Upsilon(4S)$ frame, given in units of $|V_{ub}|^2 \text{ps}^{-1}$. Predictions are based on the shape-function parameter values $m_b(\mu_*, \mu_*) = 4.63 \text{ GeV}$ and $\mu_\pi^2(\mu_*, \mu_*) = 0.2 \text{ GeV}^2$.

E_0 [GeV]	Mean	subl. SF	pert.	Total
1.9	27.74	± 0.36	+2.17 -1.83	+2.20 -1.87
2.0	21.42	± 0.40	+1.56 -1.34	+1.61 -1.39
2.1	15.29	± 0.45	+1.00 -0.87	+1.10 -0.98
2.2	9.68	± 0.61	+0.55 -0.48	+0.82 -0.78
2.3	5.12	± 0.77	+0.25 -0.21	+0.81 -0.80
2.4	2.05	± 0.63	+0.09 -0.07	+0.64 -0.64

state cannot have an invariant mass larger than M_D . For this ideal cut $E_l \gtrsim 2.31 \text{ GeV}$ we find with the default set of subleading shape functions (50) and renormalization scales

$$\begin{aligned} & \Gamma_u^{(0)} + (\Gamma_u^{\text{kin}(1)} + \Gamma_u^{\text{hadr}(1)}) + (\Gamma_u^{\text{kin}(2)} + \Gamma_u^{\text{hadr}(2)}) \\ &= [8.146 + (0.588 - 3.702) + (0.064 - 0.746)] |V_{ub}|^2 \text{ps}^{-1}. \end{aligned} \quad (56)$$

We note that the corrections from subleading shape functions are quite sizable. This has already been observed in [21, 22, 23]. Also, we note that the sum $\Gamma_u^{\text{kin}(1)} + \Gamma_u^{\text{kin}(2)}$ is an excellent approximation to the exact result $0.645 |V_{ub}|^2 \text{ps}^{-1}$ when using (28).

In practice, the cut can be relaxed to some extent, because the background is well understood. Tables 1 and 3 summarize our findings. The columns have the following meaning: “Mean” denotes the prediction for the partial decay rate Γ_u , “subl. SF” the uncertainty from subleading shape functions, “pert.” the perturbative uncertainties, and in the column “Total” we added the stated errors in quadrature. Note that the leading shape-function uncertainty is not included, because we do not consider it a theoretical error. To obtain the complete

Table 3: Partial decay rate $\Gamma_u(E_0)$ for a cut on lepton energy $E_l > E_0$ in the B -meson rest frame, given in units of $|V_{ub}|^2 \text{ps}^{-1}$. Predictions are based on the shape-function parameter values $m_b(\mu_*, \mu_*) = 4.57 \text{ GeV}$ and $\mu_\pi^2(\mu_*, \mu_*) = 0.3 \text{ GeV}^2$.

E_0 [GeV]	Mean	subl. SF	pert.	Total
1.9	23.90	± 0.36	+1.82 -1.50	+1.85 -1.54
2.0	17.98	± 0.39	+1.25 -1.03	+1.31 -1.11
2.1	12.41	± 0.45	+0.76 -0.62	+0.89 -0.76
2.2	7.49	± 0.59	+0.41 -0.30	+0.72 -0.66
2.3	3.54	± 0.84	+0.18 -0.16	+0.86 -0.85
2.4	1.00	± 0.83	+0.07 -0.10	+0.84 -0.84

Table 4: Partial decay rate $\gamma \Gamma_u(E_0)$ for a cut on lepton energy $E_l > E_0$ in the $\Upsilon(4S)$ frame, given in units of $|V_{ub}|^2 \text{ps}^{-1}$. Predictions are based on the shape-function parameter values $m_b(\mu_*, \mu_*) = 4.57 \text{ GeV}$ and $\mu_\pi^2(\mu_*, \mu_*) = 0.3 \text{ GeV}^2$.

E_0 [GeV]	Mean	subl. SF	pert.	Total
1.9	23.98	± 0.36	+1.83 -1.51	+1.86 -1.55
2.0	18.15	± 0.40	+1.28 -1.05	+1.34 -1.12
2.1	12.70	± 0.45	+0.80 -0.65	+0.92 -0.79
2.2	7.91	± 0.59	+0.45 -0.34	+0.74 -0.69
2.3	4.11	± 0.75	+0.22 -0.16	+0.78 -0.76
2.4	1.60	± 0.62	+0.09 -0.09	+0.62 -0.63

theoretical uncertainty one should add the weak annihilation error in quadrature to the values in the column “Total”.

Experiments often do not measure the partial rates in the B -meson rest frame, but work at the $\Upsilon(4S)$ resonance. Boosting to the $\Upsilon(4S)$ frame with $\beta = v/c \approx 0.064$ has a small effect on the spectrum and rates. The exact formula for this boost is

$$\gamma \Gamma_u^{(\Upsilon)}(E_0) = \frac{1}{\beta_+ - \beta_-} \int_{\beta_- E_0}^{M_B/2} dE \frac{d\Gamma_u^{(B)}}{dE} \left[\beta_+ - \max\left(\beta_-, \frac{E_0}{E}\right) \right], \quad (57)$$

where $\beta_\pm = \sqrt{1 \pm \beta}/\sqrt{1 \mp \beta}$, and the factor $\gamma = 1/\sqrt{1 - \beta^2} \approx 1.002$ on the left-hand side takes the time dilation of the B -meson lifetime $\tau'_B = \gamma \tau_B$ into account. (In other words, branching fractions are Lorentz invariant.) The above formula can be accurately approximated by the first term in an expansion in β^2 , which yields [16]

$$\gamma \Gamma_u^{(\Upsilon)}(E_0) = \Gamma_u^{(B)}(E_0) - \frac{\beta^2}{6} E_0^3 \left[\frac{d}{dE} \frac{1}{E} \frac{d\Gamma_u^{(B)}}{dE} \right]_{E=E_0} + O(\beta^4), \quad (58)$$

Table 5: Partial decay rate $\Gamma_u(\Delta_P, E_0)$ for a cut on the hadronic variable $P_+ \leq \Delta_P$ and lepton energy $E_l \geq E_0$, given in units of $|V_{ub}|^2 \text{ps}^{-1}$. Predictions are based on the shape-function parameter values $m_b(\mu_*, \mu_*) = 4.63 \text{ GeV}$ and $\mu_\pi^2(\mu_*, \mu_*) = 0.2 \text{ GeV}^2$.

Δ_P [GeV]	E_0 [GeV]	Mean	subl. SF	pert.	Total
0.70	0.0	54.69	± 0.73	+3.14	+3.22
				-2.91	-2.99
0.65	0.0	51.30	± 0.96	+2.89	+3.05
				-2.71	-2.87
0.60	0.0	47.47	± 1.21	+2.64	+2.91
				-2.50	-2.78
0.55	0.0	43.19	± 1.44	+2.39	+2.79
				-2.28	-2.69
0.50	0.0	38.47	± 1.60	+2.14	+2.68
				-2.04	-2.60
0.70	1.0	48.62	± 0.56	+2.83	+2.88
				-2.62	-2.68
0.65	1.0	45.63	± 0.76	+2.60	+2.71
				-2.44	-2.56
0.60	1.0	42.25	± 0.97	+2.38	+2.57
				-2.25	-2.45
0.55	1.0	38.47	± 1.17	+2.15	+2.45
				-2.05	-2.36
0.50	1.0	34.21	± 1.41	+1.92	+2.38
				-1.84	-2.32

as long as E_0 is not too close to the kinematical endpoint (i.e., $E_0 \leq \beta_- M_B/2 \approx 2.47 \text{ GeV}$). The numerical results for the partial decay rate $\gamma \Gamma_u^{(\Upsilon)}(E_0)$ in the rest frame of the $\Upsilon(4S)$ resonance are given in Tables 2 and 4.

5.2 Integrated P_+ rate

Cutting on P_+ samples the same hadronic phase space as a cut on the charged-lepton energy, since $P_+ \leq P_l$. This means that the advantage of knowing the background for the lepton endpoint translates directly into an advantage for the P_+ spectrum [7, 10]. Theoretically, a cut on P_+ is favored over a cut on E_l because of its higher efficiency. The phase space $P_+ \leq \Delta_P$ with the ideal separator $\Delta_P = M_D^2/M_B \approx 0.66 \text{ GeV}$ contains well over half of all $\bar{B} \rightarrow X_u l^- \bar{\nu}$ events. Here we find with the default settings

$$\begin{aligned} & \Gamma_u^{(0)} + (\Gamma_u^{\text{kin}(1)} + \Gamma_u^{\text{hadr}(1)}) + (\Gamma_u^{\text{kin}(2)} + \Gamma_u^{\text{hadr}(2)}) \\ &= [59.114 + (5.697 - 12.832) + (0.435 - 0.381)] |V_{ub}|^2 \text{ps}^{-1}. \end{aligned} \quad (59)$$

We see a stronger convergence of the power series than in the charged-lepton energy endpoint, namely $59.114 - 7.135 + 0.054$ when grouping the above numbers according to their power counting. It is also a fact that the sum $\Gamma_u^{\text{kin}(1)} + \Gamma_u^{\text{kin}(2)}$ is extremely close to the full perturbative correction of $6.107 |V_{ub}|^2 \text{ps}^{-1}$.

Often times it is required to impose an additional cut on the charged-lepton energy, as leptons that are too soft are difficult to detect. In Table 5 we list results for both $E_l \geq 0$ and $E_l \geq 1.0 \text{ GeV}$. For the ideal cut we find that the prediction is quite precise, as the theoretical

Table 6: Partial decay rate $\Gamma_u(\Delta_P, E_0)$ for a cut on the hadronic variable $P_+ \leq \Delta_P$ and lepton energy $E_l \geq E_0$, given in units of $|V_{ub}|^2 \text{ps}^{-1}$. Predictions are based on the shape-function parameter values $m_b(\mu_*, \mu_*) = 4.57 \text{ GeV}$ and $\mu_\pi^2(\mu_*, \mu_*) = 0.3 \text{ GeV}^2$.

Δ_P [GeV]	E_0 [GeV]	Mean	subl. SF	pert.	Total
0.70	0.0	45.77	± 0.72	+2.49	+2.59
				-2.29	-2.40
0.65	0.0	42.78	± 0.91	+2.26	+2.44
				-2.11	-2.30
0.60	0.0	39.53	± 1.09	+2.05	+2.32
				-1.94	-2.22
0.55	0.0	36.03	± 1.23	+1.84	+2.21
				-1.76	-2.15
0.50	0.0	32.25	± 1.31	+1.64	+2.10
				-1.59	-2.06
0.70	1.0	40.60	± 0.55	+2.22	+2.29
				-2.05	-2.12
0.65	1.0	37.98	± 0.71	+2.02	+2.14
				-1.89	-2.02
0.60	1.0	35.13	± 0.87	+1.83	+2.02
				-1.73	-1.94
0.55	1.0	32.02	± 1.01	+1.64	+1.93
				-1.58	-1.87
0.50	1.0	28.55	± 1.23	+1.46	+1.91
				-1.42	-1.88

uncertainty is about 6.4%. For comparison, the ideal cut for the lepton energy is uncertain by about 36%, but rapidly improving as the energy cut is relaxed.

5.3 Hadronic M_X - q^2 cuts

The ideal separator for the discrimination of charmed events is to cut on the invariant mass M_X of the final hadronic state $M_X \leq M_D$. It has also been argued [43, 44] that a cut on q^2 can reduce the shape-function sensitivity, since the large P_- region is avoided and the P_+ integration domain is rather large. In order to optimize signal efficiency and theoretical uncertainties, a q^2 cut is often combined with a cut on hadronic invariant mass. In Tables 7 and 8 we give results for typical cuts on both variables.

Let us study the contributions for a the optimal cut $M_X \leq M_D$ in detail. We find with the default settings

$$\begin{aligned} & \Gamma_u^{(0)} + (\Gamma_u^{\text{kin}(1)} + \Gamma_u^{\text{hadr}(1)}) + (\Gamma_u^{\text{kin}(2)} + \Gamma_u^{\text{hadr}(2)}) \\ &= [63.229 + (9.513 - 9.627) + (2.750 - 0.514)] |V_{ub}|^2 \text{ps}^{-1}. \end{aligned} \quad (60)$$

Note the almost perfect cancellation of the two terms of order $1/(M_B - P_+)$, so that the power series reads $63.229 - 0.113 + 2.236$. We observe again that the sum $\Gamma_u^{\text{kin}(1)} + \Gamma_u^{\text{kin}(2)}$ is an excellent approximation to the exact value $\Gamma_u^{\text{kin}} = 11.746 |V_{ub}|^2 \text{ps}^{-1}$. The analogous analysis for a combined cut $M_X \leq 1.7 \text{ GeV}$ and $q^2 \geq 8.0 \text{ GeV}^2$ reads

$$\begin{aligned} & \Gamma_u^{(0)} + (\Gamma_u^{\text{kin}(1)} + \Gamma_u^{\text{hadr}(1)}) + (\Gamma_u^{\text{kin}(2)} + \Gamma_u^{\text{hadr}(2)}) \\ &= [28.547 + (4.925 - 7.137) + (1.879 - 0.263)] |V_{ub}|^2 \text{ps}^{-1}, \end{aligned} \quad (61)$$

Table 7: Partial decay rate $\Gamma_u(M_0, q_0^2, E_0)$ for combined hadronic cuts $M_X \leq M_0$, $q^2 > q_0^2$, and lepton energy $E_l \geq E_0$, given in units of $|V_{ub}|^2 \text{ps}^{-1}$. Predictions are based on the shape-function parameter values $m_b(\mu_*, \mu_*) = 4.63 \text{ GeV}$ and $\mu_\pi^2(\mu_*, \mu_*) = 0.2 \text{ GeV}^2$.

M_0 [GeV]	q_0^2 [GeV ²]	E_0 [GeV]	Mean	subl. SF	pert.	Total
M_D	0.0	0.0	65.35	± 0.24	+4.70 -4.06	+4.71 -4.07
1.70	0.0	0.0	58.87	± 0.67	+4.07 -3.61	+4.13 -3.67
1.55	0.0	0.0	51.20	± 1.09	+3.46 -3.13	+3.63 -3.31
M_D	6.0	0.0	38.31	± 0.24	+3.36 -2.84	+3.37 -2.85
1.70	8.0	0.0	27.95	± 0.24	+2.53 -2.18	+2.54 -2.19
M_D	$(M_B - M_D)^2$	0.0	14.85	± 0.30	+1.67 -1.42	+1.69 -1.45
M_D	0.0	1.0	58.99	± 0.12	+4.37 -3.76	+4.37 -3.76
1.70	0.0	1.0	53.52	± 0.45	+3.80 -3.35	+3.83 -3.38
1.55	0.0	1.0	46.91	± 0.82	+3.24 -2.92	+3.34 -3.04
M_D	6.0	1.0	37.76	± 0.24	+3.32 -2.81	+3.33 -2.82
1.70	8.0	1.0	27.89	± 0.24	+2.53 -2.17	+2.54 -2.19
M_D	$(M_B - M_D)^2$	1.0	14.85	± 0.30	+1.67 -1.42	+1.69 -1.45

Table 8: Partial decay rate $\Gamma_u(M_0, q_0^2, E_0)$ for combined hadronic cuts $M_X \leq M_0$, $q^2 > q_0^2$, and lepton energy $E_l \geq E_0$, given in units of $|V_{ub}|^2 \text{ps}^{-1}$. Predictions are based on the shape-function parameter values $m_b(\mu_*, \mu_*) = 4.57 \text{ GeV}$ and $\mu_\pi^2(\mu_*, \mu_*) = 0.3 \text{ GeV}^2$.

M_0 [GeV]	q_0^2 [GeV ²]	E_0 [GeV]	Mean	subl. SF	pert.	Total
M_D	0.0	0.0	56.69	± 0.27	+4.04 -3.46	+4.05 -3.47
1.70	0.0	0.0	50.15	± 0.64	+3.39 -2.98	+3.45 -3.05
1.55	0.0	0.0	43.13	± 0.94	+2.80 -2.51	+2.95 -2.69
M_D	6.0	0.0	33.48	± 0.23	+2.90 -2.43	+2.91 -2.44
1.70	8.0	0.0	23.90	± 0.23	+2.12 -1.80	+2.14 -1.81
M_D	$(M_B - M_D)^2$	0.0	12.60	± 0.30	+1.40 -1.17	+1.43 -1.21
M_D	0.0	1.0	51.24	± 0.15	+3.76 -3.20	+3.76 -3.21
1.70	0.0	1.0	45.62	± 0.43	+3.17 -2.77	+3.20 -2.80
1.55	0.0	1.0	39.49	± 0.70	+2.62 -2.35	+2.71 -2.45
M_D	6.0	1.0	32.99	± 0.23	+2.87 -2.40	+2.88 -2.41
1.70	8.0	1.0	23.84	± 0.23	+2.12 -1.80	+2.13 -1.81
M_D	$(M_B - M_D)^2$	1.0	12.60	± 0.30	+1.40 -1.17	+1.43 -1.21

which means that the power series is $28.547 - 2.211 + 1.616$ and well under control. Here, we find $\Gamma_u^{\text{kin}} = 6.400 |V_{ub}|^2 \text{ps}^{-1}$.

The lessons to learn are that the power series is well under control, that the Taylor approximation of (28) works superbly, and that we can safely neglect contributions at third order in power counting. Note that this is true even for cuts that do not necessarily involve the full extent of the shape-function region.

5.4 Cuts on s_H^{max} and E_l

In [45] the BaBar collaboration employed a cut on both $E_l \geq E_0$ and a new kinematical variable $s_H^{\text{max}} \leq s_0$, where the definition for s_H^{max} involves both hadronic and leptonic variables. In the B -meson rest frame it is

$$s_H^{\text{max}} = M_B^2 + q^2 - 2M_B E_l - 2M_B \frac{q^2}{4E_l}. \quad (62)$$

It is a non-trivial exercise to rewrite the phase space of this cut in the variables P_+, P_-, P_l . In general a two-dimensional slice for fixed P_+ branches out into two ‘‘legs’’ in the (P_-, P_l) plane. However, for lepton-energy cuts $E_0 > (M_B - \sqrt{s_0})/2 \approx 1.705 \text{ GeV}$ the structure remains simple and can be written as

$$\begin{aligned} 0 \leq P_+ &\leq \min [M_B - 2E_0, \sqrt{s_0}], \\ P_+ \leq P_- &\leq \min \left[\frac{s_0}{P_+}, M_B \right], \\ P_+ \leq P_l &\leq \text{If} \left\{ (M_B - P_+)(M_B - P_-) \geq (M_B - \sqrt{s_0})^2, \right. \\ &\quad \text{then } \min [P_-, M_B - 2E_0], \\ &\quad \left. \text{else } \min [M_B - 2E_0, P_l^{\text{max}}(P_+, P_-)] \right\}, \end{aligned} \quad (63)$$

where

$$P_l^{\text{max}}(P_+, P_-) = \left(\frac{P_+ + P_-}{2} + \frac{s_0 - P_+ P_-}{2M_B} \right) - \sqrt{\left(\frac{P_+ + P_-}{2} + \frac{s_0 - P_+ P_-}{2M_B} \right)^2 - s_0}. \quad (64)$$

A summary of our findings is given in Tables 9 and 10. When compared to the pure charged-lepton energy cut in Tables 1 and 3, the additional cut on s_H^{max} eliminates roughly another 20–30% of events. However, the hope is that this cut also reduces the sensitivity to the leading shape function, which we expect to be sizable for the pure E_l cut. The uncertainty from subleading shape functions, however, is almost unaffected by the s_H^{max} cut.

5.5 Eliminating weak annihilation contributions

In Section 3.5 we have argued that a cut on *high* q^2 , i.e., $q^2 < q_0^2$, will eliminate the effect of weak annihilation and remove the uncertainty associated with this contribution. The cutoff

Table 9: Partial decay rate $\Gamma_u(M_0, q_0^2, E_0)$ for combined cuts $s_H^{\max} \leq s_0^{\max}$, and lepton energy $E_l \geq E_0$, given in units of $|V_{ub}|^2 \text{ps}^{-1}$. Predictions are based on the shape-function parameter values $m_b(\mu_*, \mu_*) = 4.63 \text{ GeV}$ and $\mu_\pi^2(\mu_*, \mu_*) = 0.2 \text{ GeV}^2$.

s_0^{\max} [GeV ²]	E_0 [GeV]	Mean	subl. SF	pert.	Total
3.5	1.8	20.06	± 0.41	+1.78	+1.83
				-1.53	-1.59
3.5	1.9	18.28	± 0.41	+1.54	+1.59
				-1.33	-1.39
3.5	2.0	15.84	± 0.43	+1.22	+1.29
				-1.06	-1.14
3.5	2.1	12.65	± 0.46	+0.84	+0.96
				-0.74	-0.87

Table 10: Partial decay rate $\Gamma_u(M_0, q_0^2, E_0)$ for combined cuts $s_H^{\max} \leq s_0^{\max}$, and lepton energy $E_l \geq E_0$, given in units of $|V_{ub}|^2 \text{ps}^{-1}$. Predictions are based on the shape-function parameter values $m_b(\mu_*, \mu_*) = 4.57 \text{ GeV}$ and $\mu_\pi^2(\mu_*, \mu_*) = 0.3 \text{ GeV}^2$.

s_0^{\max} [GeV ²]	E_0 [GeV]	Mean	subl. SF	pert.	Total
3.5	1.8	16.98	± 0.41	+1.48	+1.53
				-1.24	-1.30
3.5	1.9	15.31	± 0.41	+1.25	+1.32
				-1.04	-1.12
3.5	2.0	13.08	± 0.43	+0.97	+1.06
				-0.80	-0.90
3.5	2.1	10.30	± 0.47	+0.67	+0.81
				-0.53	-0.71

q_0^2 should be small enough to exclude the region around $q^2 = m_b^2$, where this contribution is concentrated. It is instructive to assess the ‘‘cost’’ of such an additional cut in terms of the loss of efficiency and, more importantly, the behavior of the remaining uncertainties. We investigate the effect using the generous cut $q_0^2 = (M_B - M_D)^2$, and combine it with two other typical cuts which discriminate against charm background: M_X and P_+ . While this particular choice for q_0^2 still leaves some room to improve the efficiency by increasing q_0^2 , it is not desirable to raise the cut much further, since this would threaten the validity of quark-hadron duality.

The results are summarized in Table 11 and can be compared to the previous ‘‘pure’’ P_+ and M_X cuts in Tables 5 and 7. In order to do so, we should keep in mind that for the latter case the weak-annihilation error $\pm 1.4|V_{ub}|^2 \text{ps}^{-1}$ must be added in quadrature to the column ‘‘Total’’. As an example, let us consider the case $P_+ \leq 0.65 \text{ GeV}$, which is close to the charm threshold. Without the additional q^2 cut we found that the subleading shape-function sensitivity is about 1.9%, and the final theoretical uncertainty (including the weak-annihilation error) is $(+6.5/-6.2)\%$. This relative error is denoted by $R^{(-)}$ in the Table. When cutting in addition on $q^2 \leq (M_B - M_D)^2$ the efficiency decreases by about 20% as expected, but the subleading shape-function sensitivity increases to 2.9%. However, due to the absence of the weak annihilation uncertainty, the overall uncertainty also decreases to $R^{(+)} = (+6.0/-5.7)\%$, so that it becomes favorable to impose the additional cut from the theoretical point of view.

Table 11: Examples for partial decay rates with cuts on $q^2 \leq (M_B - M_D)^2$. We consider an additional cut on the hadronic variable $P_+ \leq \Delta_P$ (top), or on the hadronic mass $M_X \leq M_0$ (bottom). As before, decay rates are given in units of $|V_{ub}|^2 \text{ps}^{-1}$. Predictions are based on the shape-function parameter values $m_b(\mu_*, \mu_*) = 4.63 \text{ GeV}$ and $\mu_\pi^2(\mu_*, \mu_*) = 0.2 \text{ GeV}^2$. See text for the meaning of $R^{(\pm)}$.

Δ_P [GeV]	Mean	subl. SF	pert.	Total	$R^{(-)}$	$R^{(+)}$
0.70	43.78	± 0.97	+2.34 -2.14	+2.53 -2.35	+6.4 % -6.0 %	+5.8 % -5.4 %
0.65	41.02	± 1.18	+2.18 -2.01	+2.48 -2.33	+6.5 % -6.2 %	+6.0 % -5.7 %
0.60	37.90	± 1.40	+2.01 -1.87	+2.45 -2.34	+6.8 % -6.5 %	+6.5 % -6.2 %
0.55	34.41	± 1.61	+1.84 -1.71	+2.44 -2.35	+7.2 % -7.0 %	+7.1 % -6.8 %
0.50	30.57	± 1.75	+1.65 -1.54	+2.41 -2.33	+7.8 % -7.7 %	+7.9 % -7.6 %
M_0 [GeV]	Mean	subl. SF	pert.	Total	$R^{(-)}$	$R^{(+)}$
M_D	50.49	± 0.53	+3.04 -2.64	+3.09 -2.70	+7.5 % -6.6 %	+6.1 % -5.3 %
1.70	44.21	± 0.96	+2.49 -2.24	+2.67 -2.44	+7.4 % -6.7 %	+6.0 % -5.5 %
1.55	37.07	± 1.38	+2.03 -1.87	+2.46 -2.33	+7.6 % -7.0 %	+6.6 % -6.3 %

5.6 Dependence on m_b and shape-function sensitivity

It is instructive to study how the partial decay rates depend on the b -quark mass $m_b^{\text{SF}}(\mu_*, \mu_*)$. Recall that a dependence enters only via the moment constraints on the leading shape function, apart from a small sensitivity via hard matching corrections. When studying the dependence on the b -quark mass it is therefore important to also explore the dependence on the local shape of the shape function, i.e. the effect of the variation of the shape while keeping $m_b^{\text{SF}}(\mu_*, \mu_*)$ fixed. This can be done by using two different models that share the same first moments, for example the exponential and the gaussian function in (44).

To explore the dependence on m_b (which is from now on $m_b^{\text{SF}}(\mu_*, \mu_*)$) we define the exponent

$$a(m_b) = \frac{d \ln \Gamma_u}{d \ln m_b}, \quad (65)$$

which means that $\Gamma_u \sim (m_b)^{a(m_b)}$. To calculate $a(m_b)$ we construct a pair of shape-function models with slightly different values for m_b . They will give rise to slightly different results. From (65) it follows that

$$a(m_b) = \left(\frac{\Delta \Gamma}{\Gamma} \right) / \left(\frac{\Delta m_b}{m_b} \right). \quad (66)$$

In order to study the sensitivity to the functional form of the shape function, we perform this procedure for both the exponential and the gaussian shape-function models. The values of $a(m_b)$ are obtained by averaging over the results of both types.

In Table 12 the values for $a(m_b)$ are shown over a wide range of m_b . It is reassuring that $a \approx 10$ for the pure q^2 cut, in accordance with the findings of [30, 31]. We also compile the

Table 12: Values for $a(m_b)$ vs. m_b . Also quoted is the sensitivity to the shape of the shape function.

	m_b [GeV]	4.52	4.57	4.62	4.67	4.72	4.77
$M_X \leq M_D$	$a(m_b)$	9.2	8.5	8.0	7.5	7.1	6.6
	exp vs. gauss	1.3%	1.1%	0.9%	0.7%	0.5%	0.6%
$M_X \leq 1.7$ GeV, $q^2 \geq 8$ GeV ²	$a(m_b)$	10.0	9.5	9.2	8.8	8.6	8.2
	exp vs. gauss	0.6%	0.5%	0.3%	0.2%	0.2%	0.4%
$q^2 \geq (M_B - M_D)^2$	$a(m_b)$	11.1	10.9	10.7	10.6	10.4	10.1
	exp vs. gauss	0.7%	0.7%	0.7%	0.7%	0.7%	1.0%
$P_+ \leq 0.66$ GeV	$a(m_b)$	15.6	14.0	12.6	11.4	10.4	9.3
	exp vs. gauss	4.9%	4.7%	4.3%	3.8%	3.3%	3.0%
$E_l \geq 2.2$ GeV	$a(m_b)$	21.3	19.8	18.6	17.5	16.5	15.5
	exp vs. gauss	4.0%	3.7%	3.4%	3.1%	2.9%	3.0%

values for some cuts that are truly in the shape-function region, for example P_+ or E_l . For those we find very large values of $a(m_b)$ and bigger variations. However, it is important to remember that the m_b dependence enters primarily through the shape function, which is why it is helpful to also know the dependence on the shape. The interpretation is that the large dependence on m_b (via the shape function) can be, to a certain extent, compensated by the shape (of the shape function). This is true for all cuts, and most dramatically for the cuts on P_+ or E_l . We also checked that for much more relaxed cuts the value of $a(m_b)$ tends to 5, as it should. For example, for a cut $P_+ \leq \Delta_P$ we find

Δ_P [GeV]	0.6	0.8	1.0	1.2	1.4	1.6	1.8	2.0
a	13.6	9.0	6.7	5.7	5.2	5.0	4.8	4.8

at a central value $m_b(\mu_*, \mu_*) = 4.65$ GeV.

6 Conclusions

A high-precision measurement of the parameters of the unitarity triangle is an ongoing quest, which necessitates the close cooperation of theory and experiment. The determination of $|V_{ub}|$ from inclusive $\bar{B} \rightarrow X_u l^- \bar{\nu}$ requires the measurement of partial decay rates with kinematical cuts that eliminate the large background from $\bar{B} \rightarrow X_c l^- \bar{\nu}$ decays, as well as theoretical predictions for such quantities. To this end, it is desirable to have a theoretical description of the triple differential decay rate, which can be used for predicting arbitrary partial rates obtained after integrating over certain regions of phase space. One problem in providing such a description is that the power-counting rules of the heavy-quark expansion are different in different kinematical domains. In this paper we have overcome this difficulty.

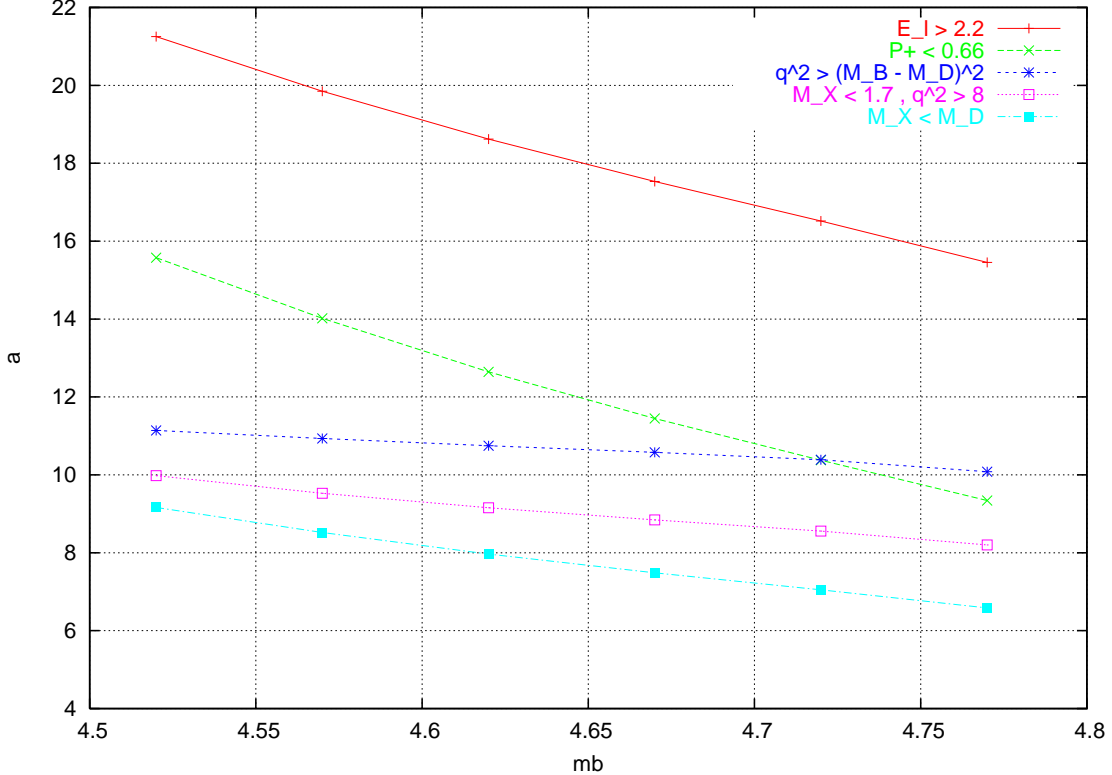


Figure 5: Values for $a(m_b)$ vs. m_b .

In the shape-function region, our results are in agreement with QCD factorization theorems, and perturbative effects have been separated from non-perturbative shape functions. When the allowed phase space extends over a large domain, our results smoothly reduce to the expressions obtained from the local operator product expansion. We have presented a formalism in which event distributions and partial decay rates are expressed without explicit reference to partonic quantities such as the b -quark mass. The sensitivity to such hadronic parameters enters indirectly, via the moments of shape functions.

The most important non-perturbative object, namely the leading-order shape function, can be extracted from the photon spectrum in $\bar{B} \rightarrow X_s \gamma$ decays, for which we have presented a detailed description analogous to our treatment of $\bar{B} \rightarrow X_u l^- \bar{\nu}$ event distributions. This is analogous to extractions of parton distribution functions from fits to data on deep inelastic scattering. In this way, the dominant uncertainty from our ignorance about bound-state effects in the B meson is turned into an experimental uncertainty, which will reduce with increasing accuracy of the experimental data on the photon spectrum. Residual hadronic uncertainties are power suppressed in the heavy-quark expansion. One goal of this paper was to present a detailed framework in which this program can be carried out. We have given formulae that can be readily used for the construction of a reliable event generator, as well as to estimate the remaining theoretical uncertainties in a robust and automated fashion.

Our theoretical expressions for the $\bar{B} \rightarrow X_s \gamma$ photon spectrum, and for the triple differ-

ential $\bar{B} \rightarrow X_u l^- \bar{\nu}$ decay rate, include state-of-the-art expressions for both perturbative and non-perturbative contributions. In the shape-function region, the decay rates are factorized into hard, jet, and shape functions at next-to-leading order in renormalization-group improved perturbation theory. Subleading shape functions are included at tree level. We also include kinematical power corrections, which are known at order α_s , as well as residual hadronic power corrections of order $1/m_b^2$.

In practice the leading shape function needs to be parameterized. We have suggested three different functional forms, which can be used to fit the data of the $\bar{B} \rightarrow X_s \gamma$ photon spectrum. Once the data is accurately described by a set of shape functions, this set can be used in the predictions for partial $\bar{B} \rightarrow X_u l^- \bar{\nu}$ rates and spectra. The spread of results for a given kinematical cut represents the leading shape-function uncertainty.

The subleading shape functions, which come in a different linear combination than in the $\bar{B} \rightarrow X_s \gamma$ case, give rise to theoretical uncertainties starting at the level of $1/m_b$ power corrections. We have estimated these uncertainties using a set of models, each of which obeys the known tree-level moment relations, but which are very different in their functional form. A second error estimate is determined by the residual renormalization-scale dependence. We also considered uncertainties from weak annihilation effects, which can be avoided by cutting away the region of phase space in which they contribute. We have suggested a cut on high lepton invariant mass, which accomplishes just that.

Numerical predictions and the theoretical errors have been assembled in the second half of this paper. We have presented results for many experimental cuts, including cuts on the charged-lepton energy (both in the rest frame of the B -meson and the $\Upsilon(4S)$ resonance), on the hadronic P_+ variable, on M_X , on q^2 , and on various combinations of these cuts. Once the data on the $\bar{B} \rightarrow X_s \gamma$ photon spectrum are sufficiently precise to accurately determine the leading-order shape function, a determination of $|V_{ub}|$ seems feasible with theory uncertainties at the 5–10% level.

Acknowledgments: We are grateful to many of our colleagues in both experiment and theory. We thank Ilija Bizjak, Riccardo Faccini, Lawrence Gibbons, Vladimir Golubev, Robert Kowalewski, Seung Lee, Zoltan Ligeti, Antonio Limosani, Francesca Di Lodovico, Vera Luth, Thomas Meyer, Masahiro Morii, Franz Muheim, and Tadao Nozaki for valuable discussions. We would like to thank the Institute for Advanced Study, Princeton, NJ, where part of this work was done, for their hospitality. The work of B.O.L. was supported in part by funds provided by the U.S. Department of Energy (D.O.E.) under cooperative research agreement DE-FC02-94ER40818. The research of M.N. and G.P. was supported by the National Science Foundation under Grant PHY-0355005.

A Perturbative Expressions

A.1 Anomalous dimensions

Here we list the known perturbative expansions of the β -function and relevant anomalous dimensions. We work in the $\overline{\text{MS}}$ scheme and define

$$\begin{aligned}\beta(\alpha_s) &= \frac{d\alpha_s(\mu)}{d\ln\mu} = -2\alpha_s \sum_{n=0}^{\infty} \beta_n \left(\frac{\alpha_s}{4\pi}\right)^{n+1}, \\ \gamma(\alpha_s) &= \sum_{n=0}^{\infty} \gamma_n \left(\frac{\alpha_s}{4\pi}\right)^{n+1}, \quad \Gamma_{\text{cusp}}(\alpha_s) = \sum_{n=0}^{\infty} \Gamma_n \left(\frac{\alpha_s}{4\pi}\right)^{n+1},\end{aligned}\tag{67}$$

as the expansion coefficients for the β -function, the leading order SCET current anomalous dimension, and the cusp anomalous dimension. To three-loop order, the β function reads

$$\begin{aligned}\beta_0 &= \frac{11}{3} C_A - \frac{2}{3} n_f, \quad \beta_1 = \frac{34}{3} C_A^2 - \frac{10}{3} C_A n_f - 2C_F n_f, \\ \beta_2 &= \frac{2857}{54} C_A^3 + \left(C_F^2 - \frac{205}{18} C_F C_A - \frac{1415}{54} C_A^2\right) n_f + \left(\frac{11}{9} C_F + \frac{79}{54} C_A\right) n_f^2,\end{aligned}\tag{68}$$

where $n_f = 4$ is the number of light flavors, $C_A = 3$ and $C_F = 4/3$. The three-loop expression for the cusp anomalous dimension has recently been obtained in [46]. The coefficients read

$$\begin{aligned}\Gamma_0 &= 4C_F, \quad \Gamma_1 = 8C_F \left[\left(\frac{67}{18} - \frac{\pi^2}{6}\right) C_A - \frac{5}{9} n_f \right], \\ \Gamma_2 &= 16C_F \left[\left(\frac{245}{24} - \frac{67\pi^2}{54} + \frac{11\pi^4}{180} + \frac{11}{6} \zeta_3\right) C_A^2 + \left(-\frac{209}{108} + \frac{5\pi^2}{27} - \frac{7}{3} \zeta_3\right) C_A n_f \right. \\ &\quad \left. + \left(-\frac{55}{24} + 2\zeta_3\right) C_F n_f - \frac{1}{27} n_f^2 \right].\end{aligned}\tag{69}$$

The SCET anomalous dimension γ is explicitly known only to one-loop order. However, the two-loop coefficient can be extracted by noting that γ is related to the axial-gauge anomalous dimension in deep-inelastic scattering [17]. The result is

$$\begin{aligned}\gamma_0 &= -5C_F, \\ \gamma_1 &= -8C_F \left[\left(\frac{3}{16} - \frac{\pi^2}{4} + 3\zeta_3\right) C_F + \left(\frac{1549}{432} + \frac{7\pi^2}{48} - \frac{11}{4} \zeta_3\right) C_A - \left(\frac{125}{216} + \frac{\pi^2}{24}\right) n_f \right].\end{aligned}\tag{70}$$

A.2 Sudakov factor

The exact expression for the Sudakov factor reads

$$\ln U(\mu_h, \mu_i) = 2S_\Gamma(\mu_h, \mu_i) - 2a_\Gamma(\mu_h, \mu_i) \ln \frac{m_b}{\mu_h} - 2a_\gamma(\mu_h, \mu_i),\tag{71}$$

where the functions of the right-hand side are solutions to the renormalization-group equations

$$\begin{aligned}\frac{d}{d \ln \mu} S_\Gamma(\nu, \mu) &= -\Gamma_{\text{cusp}}(\alpha_s(\mu)) \ln \frac{\mu}{\nu}, \\ \frac{d}{d \ln \mu} a_\Gamma(\nu, \mu) &= -\Gamma_{\text{cusp}}(\alpha_s(\mu)), \quad \frac{d}{d \ln \mu} a_\gamma(\nu, \mu) = -\gamma(\alpha_s(\mu)),\end{aligned}\quad (72)$$

with boundary conditions $S(\nu, \mu) = 0$ etc. at $\mu = \nu$. These equations can be integrated using that $d/d \ln \mu = \beta(\alpha_s) d/d\alpha_s$. The solutions are

$$S_\Gamma(\nu, \mu) = - \int_{\alpha_s(\nu)}^{\alpha_s(\mu)} d\alpha \frac{\Gamma_{\text{cusp}}(\alpha)}{\beta(\alpha)} \int_{\alpha_s(\nu)}^{\alpha} \frac{d\alpha'}{\beta(\alpha')}, \quad a_\Gamma(\nu, \mu) = - \int_{\alpha_s(\nu)}^{\alpha_s(\mu)} d\alpha \frac{\Gamma_{\text{cusp}}(\alpha)}{\beta(\alpha)}, \quad (73)$$

and similarly for a_γ .

Next, we give explicit results for the Sudakov function S_Γ and the functions a_Γ and a_γ in (71) at next-to-leading order in renormalization-group improved perturbation theory. We obtain

$$a_\Gamma(\nu, \mu) = \frac{\Gamma_0}{2\beta_0} \left[\ln \frac{\alpha_s(\mu)}{\alpha_s(\nu)} + \left(\frac{\Gamma_1}{\Gamma_0} - \frac{\beta_1}{\beta_0} \right) \frac{\alpha_s(\mu) - \alpha_s(\nu)}{4\pi} + \dots \right], \quad (74)$$

and similarly for a_γ . The Sudakov factor S_Γ requires the knowledge of the three-loop coefficients β_2 and Γ_2 and reads with $r = \alpha_s(\mu)/\alpha_s(\nu)$

$$\begin{aligned}S_\Gamma(\nu, \mu) &= \frac{\Gamma_0}{4\beta_0^2} \left\{ \frac{4\pi}{\alpha_s(\nu)} \left(1 - \frac{1}{r} - \ln r \right) + \left(\frac{\Gamma_1}{\Gamma_0} - \frac{\beta_1}{\beta_0} \right) (1 - r + \ln r) + \frac{\beta_1}{2\beta_0} \ln^2 r \right. \\ &\quad + \frac{\alpha_s(\nu)}{4\pi} \left[\left(\frac{\beta_1 \Gamma_1}{\beta_0 \Gamma_0} - \frac{\beta_2}{\beta_0} \right) (1 - r + r \ln r) + \left(\frac{\beta_1^2}{\beta_0^2} - \frac{\beta_2}{\beta_0} \right) (1 - r) \ln r \right. \\ &\quad \left. \left. - \left(\frac{\beta_1^2}{\beta_0^2} - \frac{\beta_2}{\beta_0} - \frac{\beta_1 \Gamma_1}{\beta_0 \Gamma_0} + \frac{\Gamma_2}{\Gamma_0} \right) \frac{(1 - r)^2}{2} \right] + \dots \right\}. \quad (75)\end{aligned}$$

The next-to-leading-logarithmic Sudakov factor $U(\mu_h, \mu_i)$ can be obtained by combining the above expressions according to (71) and expanding out terms of order α_s .

B Partially integrated decay rate

With the exception of the combined cut on the lepton energy E_l and the hadronic quantity s_H^{max} studied in Section 5.4 the triple differential decay rate (21) can be integrated over the lepton energy $E_l \geq E_0$ and $P_- \leq P_-^{\text{max}}$ analytically. The quantities E_0 and P_-^{max} may depend on the value of P_+ , and the last integration over P_+ is then performed numerically. In this section we present the partially integrated decay rate

$$d\Gamma(P_+) = \int dP_l dP_- \frac{d^3\Gamma_u}{dP_l dP_- dP_+}. \quad (76)$$

In the previous discussions we have changed variables from P_- to y , defined in (23). The constraint $P_- \leq P_-^{\max}$ then translates into the integration domain $0 \leq y \leq y_0$. In close analogy to (23) we define

$$y_0 = \frac{P_-^{\max} - P_+}{M_B - P_+}, \quad \varepsilon_0 = \frac{P_l^{\max} - P_+}{M_B - P_+} = 1 - \frac{2E_0}{M_B - P_+}. \quad (77)$$

Again, the quantities y_0 and ε_0 are allowed to depend on P_+ . From the phase space (2) it follows that a cut on the lepton energy has no effect if $\varepsilon_0 \geq y_0$. In general, we can state the result as

$$d\Gamma(P_+, y_0, \varepsilon_0) = \begin{cases} d\Gamma_A(P_+, y_0) & ; \quad y_0 \leq \varepsilon_0 \\ d\Gamma_A(P_+, \varepsilon_0) + d\Gamma_B(P_+, y_0, \varepsilon_0) - d\Gamma_B(P_+, \varepsilon_0, \varepsilon_0) & ; \quad y_0 > \varepsilon_0 \end{cases} \quad (78)$$

where we distinguish between type “A”, which is independent on ε_0 , and type “B”, which carries all the ε_0 dependence. From the exact expression for the triple differential decay rate (21) it follows that the partially integrated decay rate can be written as

$$d\Gamma_A(P_+, y_0) = \frac{G_F^2 |V_{ub}|^2}{96\pi^3} U(\mu_h, \mu_i) (M_B - P_+)^5 \left[\mathcal{K}_1^{(A)}(P_+, y_0) + 6\mathcal{K}_2^{(A)}(P_+, y_0) + 2\mathcal{K}_3^{(A)}(P_+, y_0) \right], \quad (79)$$

and similarly $d\Gamma_B(P_+, y_0, \varepsilon_0)$ with $\mathcal{K}_i^{(A)}(P_+, y_0)$ replaced by $\mathcal{K}_i^{(B)}(P_+, y_0, \varepsilon_0)$. In the following we give results for the functions \mathcal{K}_i based on the previously discussed structures \mathcal{F}_i and strictly expanded in inverse powers of $(M_B - P_+)$.

The integration over y gives rise to a set of master integrals $I_n(b, y_0)$, which are explicitly given in equation (86) of [7]. They always come in certain linear combinations which are determined by the prefactors to the structure functions \mathcal{F}_i in (21) and contain all information on the lepton energy for the integration over P_l . The results can be written in a compact form by defining

$$\begin{aligned} A_n^{(k)}(y_0) &= 3I_n(3 - k - 2a_\Gamma, y_0) - 2I_n(4 - k - 2a_\Gamma, y_0), \\ B_n^{(k)}(y_0, \varepsilon_0) &= \varepsilon_0 \left[-6I_n(3 - k - 2a_\Gamma, y_0) + 6(1 + \varepsilon_0)I_n(2 - k - 2a_\Gamma, y_0) \right. \\ &\quad \left. - \varepsilon_0(3 + 2\varepsilon_0)I_n(1 - k - 2a_\Gamma, y_0) \right] \\ C_n^{(k)}(y_0) &= I_n(k - 2a_\Gamma, y_0), \\ D_n^{(k)}(y_0, \varepsilon_0) &= \varepsilon_0^2 \left[3I_n(k - 2 - 2a_\Gamma, y_0) - 2\varepsilon_0 I_n(b - 3 - 2a_\Gamma, y_0) \right]. \end{aligned} \quad (80)$$

It is also helpful to normalize these expressions in a particular, but to an extent arbitrary way, by defining

$$\begin{aligned} a_n^{(k)}(y_0) &= \frac{A_n^{(k)}(y_0)}{A_1^{(1)}(y_0)}, & b_n^{(k)}(y_0, \varepsilon_0) &= \frac{B_n^{(k)}(y_0, \varepsilon_0)}{B_1^{(1)}(y_0, \varepsilon_0)}, \\ c_n^{(k)}(y_0) &= \frac{C_n^{(k)}(y_0)}{C_1^{(2)}(y_0)}, & d_n^{(k)}(y_0, \varepsilon_0) &= \frac{D_n^{(k)}(y_0, \varepsilon_0)}{D_1^{(2)}(y_0, \varepsilon_0)}. \end{aligned} \quad (81)$$

Finally we also introduce abbreviations for a few integrals over the shape function $\mathcal{S}(\hat{\omega})$, which help to write the results in a more compact form. These new functions only depend on P_+ and are defined as

$$\begin{aligned}
\xi_2(P_+) &= \int_0^{P_+} d\hat{\omega} \left[\frac{1}{P_+ - \hat{\omega}} \right]_*^{[\mu_i^2/m_b]} \mathcal{S}(\hat{\omega}), \\
\xi_3(P_+) &= \int_0^{P_+} d\hat{\omega} \left[\frac{1}{P_+ - \hat{\omega}} \ln \frac{m_b(P_+ - \hat{\omega})}{\mu_i^2} \right]_*^{[\mu_i^2/m_b]} \mathcal{S}(\hat{\omega}), \\
\xi_4(P_+) &= \int_0^{P_+} d\hat{\omega} \mathcal{S}(\hat{\omega}), \\
\xi_5(P_+) &= \int_0^{P_+} d\hat{\omega} \mathcal{S}(\hat{\omega}) \ln \frac{M_B - P_+}{P_+ - \hat{\omega}}, \\
\xi_6(P_+) &= \int_0^{P_+} d\hat{\omega} (P_+ - \hat{\omega}) \mathcal{S}(\hat{\omega}), \\
\xi_7(P_+) &= \int_0^{P_+} d\hat{\omega} (P_+ - \hat{\omega}) \mathcal{S}(\hat{\omega}) \ln \frac{M_B - P_+}{P_+ - \hat{\omega}}.
\end{aligned} \tag{82}$$

The first two structures $\xi_2(P_+)$ and $\xi_3(P_+)$ appear together with $\mathcal{S}(P_+)$ in the leading power predictions. Next, $\xi_{4,5}(P_+)$ arise at subleading power in the NLO perturbative expressions (30). Finally $\xi_{6,7}(P_+)$ enter the NNLO perturbative formulae (31).

All ingredients are now in place to give expressions for $d\Gamma_A(P_+, y_0)$ and $d\Gamma_B(P_+, y_0, \varepsilon_0)$. For the first structure function \mathcal{K}_1 we find

$$\begin{aligned}
\mathcal{K}_1^{(A)}(P_+, y_0) = & A_1^{(1)}(y_0) \left[\left\{ 1 + \frac{\alpha_s(\mu_h)C_F}{4\pi} \left[(-4 \ln^2 \frac{m_b}{\mu_h} + 10 \ln \frac{m_b}{\mu_h} - \frac{\pi^2}{6} - 12) \right. \right. \right. \\
& \left. \left. \left. + (6 - 8 \ln \frac{m_b}{\mu_h}) a_2^{(1)}(y_0) - 4a_3^{(1)}(y_0) - 2a_4^{(1)}(y_0) - 4a_5^{(1)}(y_0) \right] \right. \right. \\
& \left. \left. + \frac{\alpha_s(\mu_i)C_F}{4\pi} \left[(7 - \pi^2) - 3a_2^{(1)}(y_0) + 2a_3^{(1)}(y_0) \right] \right\} \mathcal{S}(P_+) \right. \\
& \left. + \frac{\alpha_s(\mu_i)C_F}{4\pi} \left\{ \left[-3 + 4a_2^{(1)}(y_0) \right] \xi_2(P_+) + 4\xi_3(P_+) \right\} \right] \\
& + \frac{A_1^{(1)}(y_0)}{(M_B - P_+)} \left[-(\bar{\Lambda} - P_+) \mathcal{S}(P_+) + 2\hat{t}(P_+) - \{\hat{u}(P_+) - \hat{v}(P_+)\} \left(1 - a_1^{(2)}(y_0) \right) \right] \\
& + \frac{\alpha_s(\bar{\mu})C_F}{4\pi} \frac{A_1^{(1)}(y_0)}{(M_B - P_+)} \left[-\left(4 - 12a_1^{(2)}(y_0) \right) \xi_5(P_+) \right. \\
& \left. + \left(6 - 5a_1^{(2)}(y_0) + 12a_2^{(2)}(y_0) - 4a_2^{(1)}(y_0) \right) \xi_4(P_+) \right] \\
& + \frac{\alpha_s(\bar{\mu})C_F}{4\pi} \frac{A_1^{(1)}(y_0)}{(M_B - P_+)^2} \left[\left\{ -12 + 16a_1^{(2)}(y_0) + 3a_1^{(3)}(y_0) \right. \right. \\
& \left. \left. + 12a_2^{(3)}(y_0) - 20a_2^{(2)}(y_0) + 6a_2^{(1)}(y_0) \right\} \xi_6(P_+) \right. \\
& \left. + \left\{ 6 - 20a_1^{(2)}(y_0) + 12a_1^{(3)}(y_0) \right\} \xi_7(P_+) \right] \\
& + \frac{A_1^{(1)}(y_0)}{(M_B - P_+)^2} \left[-\frac{5\lambda_1 + 15\lambda_2}{6} + \frac{4\lambda_1 - 6\lambda_2}{3} a_1^{(3)}(y_0) \right] \mathcal{S}(P_+), \tag{84}
\end{aligned}$$

and similarly for $\mathcal{K}_1^{(B)}(P_+, y_0, \varepsilon_0)$ with $A_1^{(1)}(y_0)$ replaced by $B_1^{(1)}(y_0, \varepsilon_0)$ and $a_n^{(k)}(y_0)$ replaced

by $b_n^{(k)}(y_0, \varepsilon_0)$. The second structure reads

$$\begin{aligned}
\mathcal{K}_2^{(A)}(P_+, y_0) &= \frac{\alpha_s(\bar{\mu})C_F}{4\pi} \frac{1}{(M_B - P_+)} \left[C_1^{(1)}(y_0) - C_1^{(2)}(y_0) \right] \xi_4(P_+) \\
&+ \frac{\alpha_s(\bar{\mu})C_F}{4\pi} \frac{1}{(M_B - P_+)^2} \left[\left\{ 7C_1^{(0)}(y_0) - 5C_1^{(1)}(y_0) - C_1^{(2)}(y_0) - C_1^{(3)}(y_0) \right. \right. \\
&\quad \left. \left. - 4 \left(C_2^{(0)}(y_0) - C_2^{(1)}(y_0) \right) \right\} \xi_6(P_+) - 4 \left\{ C_1^{(0)}(y_0) - C_1^{(1)}(y_0) \right\} \xi_7(P_+) \right] \\
&+ \frac{1}{(M_B - P_+)^2} \left[\left\{ C_1^{(0)}(y_0) - C_1^{(1)}(y_0) \right\} \left(-\frac{2\lambda_1}{3} + \lambda_2 \right) \right] \mathcal{S}(P_+), \tag{85}
\end{aligned}$$

and similarly for $\mathcal{K}_2^{(B)}(P_+, y_0, \varepsilon_0)$ with $C_n^{(k)}(y_0)$ replaced by $\varepsilon_0 C_n^{(k-1)}(y_0)$. Finally

$$\begin{aligned}
\mathcal{K}_3^{(A)}(P_+, y_0) &= \frac{\alpha_s(\mu_h)C_F}{4\pi} \left[C_4^{(3)}(y_0) \mathcal{S}(P_+) \right] \\
&+ \frac{C_1^{(2)}(y_0)}{(M_B - P_+)} \left[-(\bar{\Lambda} - P_+) \mathcal{S}(P_+) - 2\hat{t}(P_+) + \{\hat{t}(P_+) + \hat{v}(P_+)\} c_1^{(1)}(y_0) \right] \\
&+ \frac{\alpha_s(\bar{\mu})C_F}{4\pi} \frac{C_1^{(2)}(y_0)}{(M_B - P_+)} \left[4\xi_5(P_+) + \left\{ -11 + 2c_1^{(3)}(y_0) + 4c_2^{(2)}(y_0) \right\} \xi_4(P_+) \right] \\
&+ \frac{\alpha_s(\bar{\mu})C_F}{4\pi} \frac{C_1^{(2)}(y_0)}{(M_B - P_+)^2} \left[\left\{ -14 + 26c_1^{(1)}(y_0) \right\} \xi_7(P_+) \right. \\
&\quad \left. \left\{ \frac{69}{2} - 32c_1^{(1)}(y_0) - 3c_1^{(3)}(y_0) + 26c_2^{(1)}(y_0) - 14c_2^{(2)}(y_0) \right\} \xi_6(P_+) \right] \\
&+ \frac{C_1^{(2)}(y_0)}{(M_B - P_+)^2} \left[-\frac{7\lambda_1 + 18\lambda_2}{6} + \frac{2\lambda_1 + 12\lambda_2}{3} c_1^{(1)}(y_0) \right], \tag{86}
\end{aligned}$$

and similarly for $\mathcal{K}_3^{(B)}(P_+, y_0, \varepsilon_0)$ with $C_n^{(k)}(y_0)$ replaced by $D_n^{(k)}(y_0, \varepsilon_0)$ and $c_n^{(k)}(y_0)$ replaced by $d_n^{(k)}(y_0, \varepsilon_0)$. Each line in the above formulae can be easily identified as coming from one of the contributions to \mathcal{F}_i studied in Section 3.

As an example, we can now calculate the partial decay rate for a combined cut $E_l \geq E_0$, $q^2 \geq q_0^2$, $M_X^2 \leq s_0$ by applying the above formulae for $d\Gamma(P_+, y_0, \varepsilon_0)$ with

$$y_0 = \min \left(1 - \frac{q_0^2}{(M_B - P_+)^2}, \frac{s_0 - P_+^2}{P_+(M_B - P_+)} \right), \quad \varepsilon_0 = 1 - \frac{2E_0}{M_B - P_+}, \tag{87}$$

and integrating P_+ over the interval $[0, \min(\sqrt{s_0}, M_B - \sqrt{q_0^2})]$.

References

- [1] B. Aubert *et al.* [BaBar Collaboration], Phys. Rev. Lett. **89**, 201802 (2002) [hep-ex/0207042]; K. Abe *et al.* [Belle Collaboration], hep-ex/0308036.
- [2] M. Neubert, Phys. Rev. D **49**, 3392 (1994) [hep-ph/9311325].
- [3] M. Neubert, Phys. Rev. D **49**, 4623 (1994) [hep-ph/9312311].
- [4] I. I. Y. Bigi, M. A. Shifman, N. G. Uraltsev and A. I. Vainshtein, Int. J. Mod. Phys. A **9**, 2467 (1994) [hep-ph/9312359].
- [5] G. P. Korchemsky and G. Sterman, Phys. Lett. B **340**, 96 (1994) [hep-ph/9407344].
- [6] C. W. Bauer and A. V. Manohar, Phys. Rev. D **70**, 034024 (2004) [hep-ph/0312109].
- [7] S. W. Bosch, B. O. Lange, M. Neubert and G. Paz, Nucl. Phys. B **699**, 335 (2004) [hep-ph/0402094].
- [8] A. V. Manohar and M. B. Wise, Phys. Rev. D **49**, 1310 (1994) [hep-ph/9308246].
- [9] B. Blok, L. Koyrakh, M. A. Shifman and A. I. Vainshtein, Phys. Rev. D **49**, 3356 (1994) [Erratum-ibid. D **50**, 3572 (1994)] [hep-ph/9307247].
- [10] S. W. Bosch, B. O. Lange, M. Neubert and G. Paz, Phys. Rev. Lett. **93**, 221801 (2004) [hep-ph/0403223].
- [11] S. W. Bosch, M. Neubert and G. Paz, JHEP **0411**, 073 (2004) [hep-ph/0409115].
- [12] K. G. Chetyrkin, M. Misiak and M. Munz, Phys. Lett. B **400**, 206 (1997) [Erratum-ibid. B **425**, 414 (1998)] [hep-ph/9612313].
- [13] F. De Fazio and M. Neubert, JHEP **9906**, 017 (1999) [hep-ph/9905351].
- [14] C. Greub, T. Hurth and D. Wyler, Phys. Rev. D **54**, 3350 (1996) [hep-ph/9603404].
- [15] A. Ali and C. Greub, Phys. Lett. B **361**, 146 (1995) [hep-ph/9506374].
- [16] A. L. Kagan and M. Neubert, Eur. Phys. J. C **7**, 5 (1999) [hep-ph/9805303].
- [17] M. Neubert, Eur. Phys. J. C **40**, 165 (2005) [hep-ph/0408179].
- [18] R. J. Hill, T. Becher, S. J. Lee and M. Neubert, JHEP **0407**, 081 (2004) [hep-ph/0404217].
- [19] T. Becher, R. J. Hill, B. O. Lange and M. Neubert, Phys. Rev. D **69**, 034013 (2004) [hep-ph/0309227].
- [20] C. W. Bauer, M. E. Luke and T. Mannel, Phys. Rev. D **68**, 094001 (2003) [hep-ph/0102089].
- [21] C. W. Bauer, M. Luke and T. Mannel, Phys. Lett. B **543**, 261 (2002) [hep-ph/0205150].

- [22] A. K. Leibovich, Z. Ligeti and M. B. Wise, Phys. Lett. B **539**, 242 (2002) [hep-ph/0205148].
- [23] M. Neubert, Phys. Lett. B **543**, 269 (2002) [hep-ph/0207002].
- [24] K. S. M. Lee and I. W. Stewart, hep-ph/0409045.
- [25] M. Beneke, F. Campanario, T. Mannel and B. D. Pecjak, hep-ph/0411395.
- [26] A. F. Falk and M. Neubert, Phys. Rev. D **47**, 2965 (1993) [hep-ph/9209268].
- [27] G. Martinelli, M. Neubert and C. T. Sachrajda, Nucl. Phys. B **461**, 238 (1996) [hep-ph/9504217].
- [28] M. Neubert, Phys. Lett. B **393**, 110 (1997) [hep-ph/9610471].
- [29] A. F. Falk, M. E. Luke and M. J. Savage, Phys. Rev. D **49**, 3367 (1994) [hep-ph/9308288].
- [30] M. Neubert, JHEP **0007**, 022 (2000) [hep-ph/0006068].
- [31] M. Neubert and T. Becher, Phys. Lett. B **535**, 127 (2002) [hep-ph/0105217].
- [32] N. Uraltsev, Int. J. Mod. Phys. A **14**, 4641 (1999) [hep-ph/9905520].
- [33] I. I. Y. Bigi and N. G. Uraltsev, Nucl. Phys. B **423**, 33 (1994) [hep-ph/9310285].
- [34] M. Neubert and C. T. Sachrajda, Nucl. Phys. B **483**, 339 (1997) [hep-ph/9603202].
- [35] M. B. Voloshin, Phys. Lett. B **515**, 74 (2001) [hep-ph/0106040].
- [36] Thomas Oliver Meyer, “Limits on weak annihilation in inclusive charmless semileptonic B decays”, PhD Thesis, Cornell University, (2005).
- [37] B. Aubert *et al.* [BaBar Collaboration], Phys. Rev. Lett. **93**, 011803 (2004) [hep-ex/0404017].
- [38] M. Beneke, Phys. Lett. B **434**, 115 (1998) [hep-ph/9804241].
- [39] A. H. Hoang, Z. Ligeti and A. V. Manohar, Phys. Rev. D **59**, 074017 (1999) [hep-ph/9811239].
- [40] I. I. Y. Bigi, M. A. Shifman, N. Uraltsev and A. I. Vainshtein, Phys. Rev. D **56**, 4017 (1997) [hep-ph/9704245].
- [41] M. Neubert, Phys. Lett. B **612**, 13 (2005) [hep-ph/0412241].
- [42] M. Neubert, hep-ph/0411027.
- [43] C. W. Bauer, Z. Ligeti and M. E. Luke, Phys. Lett. B **479**, 395 (2000) [hep-ph/0002161].
- [44] C. W. Bauer, Z. Ligeti and M. E. Luke, Phys. Rev. D **64**, 113004 (2001) [hep-ph/0107074].

- [45] B. Aubert *et al.* [BaBar Collaboration], hep-ex/0408045.
- [46] S. Moch, J. A. M. Vermaseren and A. Vogt, Nucl. Phys. B **688**, 101 (2004) [hep-ph/0403192].